Processes controlling magma fertility at buenavista del cobre porphyry copper deposit (cananea, méxico): A new petrogenetic model based on zircon u-pb dating and apatite geochemistry

Víctor Almada-Gutiérrez, Mélanie Noury, Thierry Calmus, Nathan Cogné, Edgardo Barrera-Moreno, Marc Poujol

Ore Geology Reviews 175 (2024) 106320

Contents lists available at ScienceDirect

Ore Geology Reviews

journal homepage: www.elsevier.com/locate/oregeorev

Processes controlling magma fertility at Buenavista del Cobre porphyry copper deposit (Cananea, México): A new petrogenetic model based on zircon U-Pb dating and apatite geochemistry

Víctor Almada-Gutiérrez [a,b,c], Mélanie Noury [a,c,*], Thierry Calmus [a,c], Nathan Cogné [d], Edgardo Barrera-Moreno [e], Marc Poujol [d]

[a] Estación Regional del Noroeste, Instituto de Geología, Universidad Nacional Autónoma de México, Hermosillo, Sonora, México
[b] Posgrado en Ciencias de la Tierra, Estación Regional del Noroeste, Instituto de Geología, Universidad Nacional Autónoma de México, Hermosillo, Sonora, México
[c] Laboratorio Nacional de Geoquímica y Mineralogía (LANGEM), Instituto de Geología, Universidad Nacional Autónoma de México, Hermosillo, Sonora, México
[d] Univ. Rennes, CNRS, Géosciences Rennes, UMR6118, F-35000 Rennes, France
[e] Buenavista del Cobre, Superintendencia de Geología, Grupo México, Cananea, Sonora, México

ARTICLE INFO

Keywords:
Porphyry copper deposit
Magma fertility
Apatite geochemistry
Geochronology
Cananea mine
Mexico

ABSTRACT

The Buenavista del Cobre is a world-class porphyry Cu-Mo deposit located in the Cananea Mining District, northern Sonora, México. Using zircon U-Pb dating, we show that the Proterozoic Cananea Granite, unconformably overlain regionally by Paleozoic limestones hosting skarn deposits underlies the present-day pit. We also present new crystallization ages for host rocks of copper mineralization in the District, dating for the first time a volcanic rock of the Henrietta Formation at 186.8 ± 1.1/3.0 Ma and the El Torre Syenite at 176.3 ± 1.1/2.9 Ma. Zircon U-Pb dating of the different porphyritic bodies reveals that the magmatic activity at Buenavista del Cobre lasted at least 4 Myr, from 59.7 ± 0.5/1.1 Ma to 56.1 ± 0.2/0.9 Ma. The deposit is composed by several porphyry intrusions referred to as "ore-rich" and "ore-poor" based on their individual metal contributions, which provides the opportunity to study the origin and processes enhancing magma fertility in an individual deposit. Combining our new geochronological dataset with geochemistry of apatite from the different porphyries allows us to propose a new petrogenetic model for the Buenavista del Cobre deposit. As the apatite Eu and Ce anomalies overlap with no clear difference between the ore-rich and ore-poor intrusions, we propose that the magmatic oxidation states of the magmas were similar. However, differences in apatite REE signatures, as well as variations in apatite Sr compositions between the two groups suggest that fractional crystallization processes in the parental magma influence the fertility of the porphyries. Additionally, apatite Cl contents of ore-rich porphyry intrusions are higher (>0.4 wt%) than the ore-poor intrusions (<0.2 wt%), suggesting an important role of the initial Cl content of the magmas in the mineralization process. These observations give new insights on the petrogenetic processes at origin of porphyry magma fertility. We propose that the evolution of the parental melt by fractional crystallization of hydrous minerals (hornblende) at upper crustal levels induced low H_2O content of the residual magma, resulting in the formation of ore-poor porphyries. In contrast, we suggest that fractionation of anhydrous minerals (plagioclase) increased the H_2O content in the residual melt, leading to the formation of ore-rich porphyries. Our new data allow us to propose an original genetic model for the Buenavista del Cobre deposit, which involves two cycles of supply, cooling and partial crystallization. This contribution shows that petrogenetic processes controlling porphyry copper magmas fertility are recorded in the composition of apatite at the deposit scale and highlights the importance of considering apatite geochemistry as an exploration tool.

1. Introduction

Porphyry copper deposits around the world are commonly associated with subduction-related magmatism and are typically the product of superposition of multiple porphyry intrusions (e.g., Proffett, 2003; Sillitoe, 2010). Zircon U-Pb geochronology studies indicate that the time span for the emplacement of porphyry intrusions in some giant deposits is ~ 2 to ~ 5 Myr (e.g., Ballard et al., 2001; Maksaev et al., 2004; Harris

* Corresponding author.
E-mail address: mnoury@geologia.unam.mx (M. Noury).

https://doi.org/10.1016/j.oregeorev.2024.106320
Received 17 May 2024; Received in revised form 24 September 2024; Accepted 29 October 2024
Available online 2 November 2024

et al., 2008). At the deposit scale, each porphyry intrusion contributes to the total metal budget of the deposit and are often labelled as "ore-rich" or "ore-poor" intrusions based on their individual metal contribution. Fertility of an intrusion is believed to be controlled by the oxidation state and by the H_2O and volatile contents of the magma (Richards, 2003 and 2011; Sillitoe, 2010). The influence of these parameters on magma fertility has been tested by analyzing and comparing ore-related versus ore-barren intrusions on a global and regional scale (e.g., Lang and Titley 1998; Loucks 2014). However, at the deposit scale, the processes controlling the fertility of the different porphyry intrusions at the origin of ore-poor and ore-rich intrusions remain unclear.

The Buenavista del Cobre deposit (formerly Cananea mine) is a world-class porphyry Cu-Mo deposit located in the center of the Cananea Mining District in northern Sonora, Mexico (Fig. 1). It is the largest Cu/Mo producer in the district with tonnages of 7,140 Mt grading 0.42 % Cu and 0.008 % Mo (Singer et al., 2005). The Cananea Mining District is part of the Arizona-Sonora-New Mexico cluster of porphyry Cu deposits, which were emplaced from the Late Cretaceous to the Eocene (Keith and Swan, 1995; Leveille and Stegen, 2012; Valencia-Moreno et al., 2016; Fig. 1). Several porphyry phases have been recognized in the Buenavista del Cobre deposit, which are distinguished by their cross-cutting relationships, mineralogical compositions and textures (Valentine, 1936; Ochoa-Landín and Echávarri-Pérez, 1978; Ochoa-Landín and Navarro-Mayer, 1979). It has been long recognized that some of these intrusions have a more important metal contribution than others and were therefore labelled as either ore-rich or ore-poor porphyry intrusions (Ochoa-Landín and Navarro-Mayer, 1979). In particular, the La Colorada and 755 porphyries are associated with significant contributions of Cu and Mo sulfides to the porphyry system (Ochoa-Landín and Navarro-Mayer, 1979; Correa-García, 1983). On the other hand, the Feldspar and 8–110 porphyries are associated with low-Cu grade breccias and the Coarse-grained Porphyry unit is referenced as "barren" (Ochoa-Landín and Navarro-Mayer, 1979; Correa-García, 1983), but presents scarce sulfide mineralization. In the following, we thus refer to the La Colorada

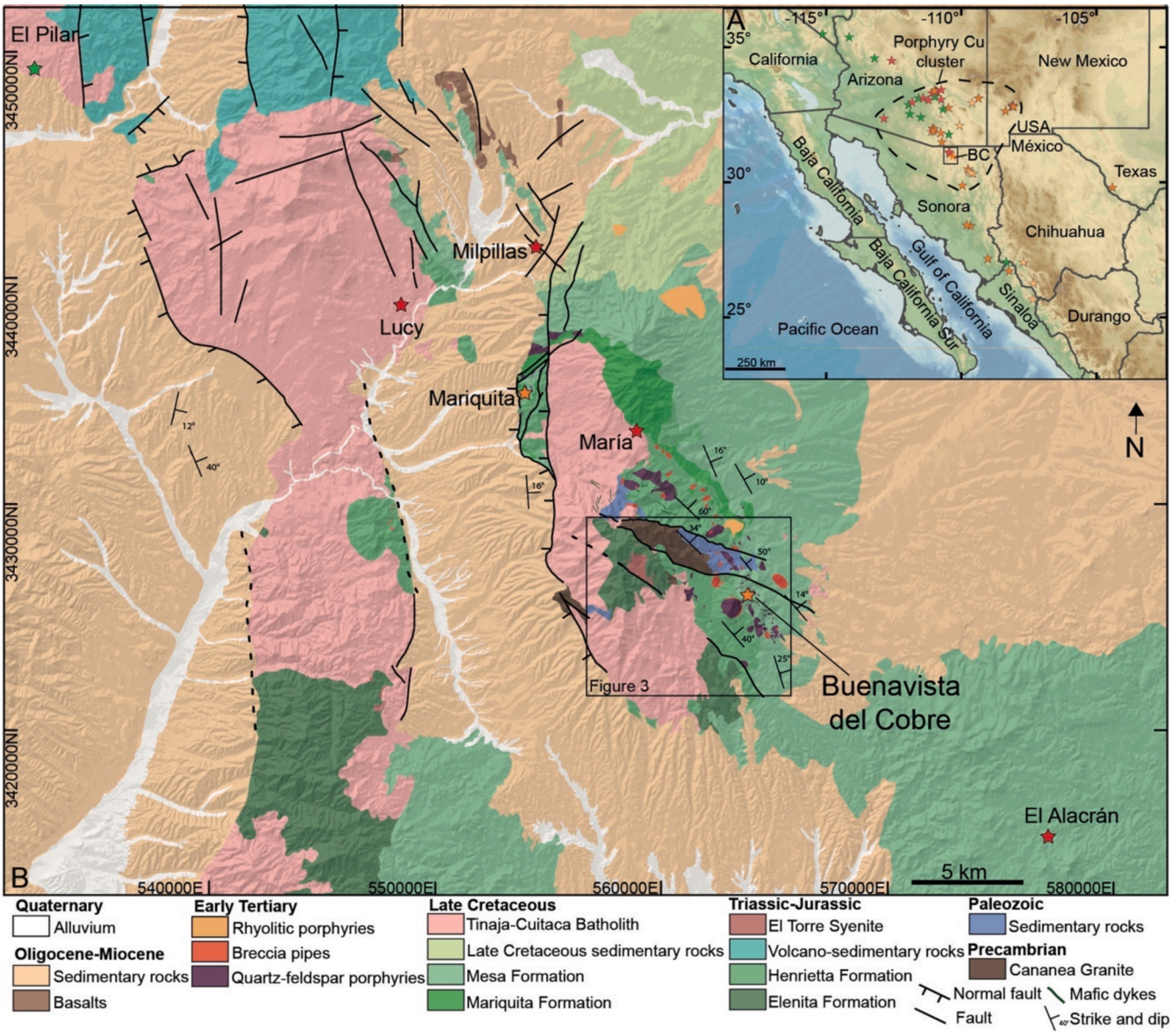

Fig. 1. Location and regional geological setting of the Cananea Mining District. Stars indicate the location of the main porphyry copper deposits, their colors corresponding to the age ranges of emplacement: green = 75–65 Ma, red = 65–60 Ma, orange = 60–55 Ma, and yellow = 55–40 Ma. A) Porphyry Cu deposits province of southwestern North America. Dotted lines indicate the limit of the porphyry copper cluster of Arizona-Sonora-New Mexico (after Del Rio Salas et al., 2017). BC = Buenavista del Cobre deposit. B) Regional geological map of the Cananea Mining District, modified from Noguez-Alcántara (2008) and Del Rio-Salas et al. (2017).

and 755 porphyries as "ore-rich intrusions" and to the Feldspar, 8–110 and Coarse-grained porphyries as "ore-poor intrusions". A comparison of the geochemical characteristics of "ore-poor" and "ore-rich" intrusions at Buenavista del Cobre can provide insights into the petrogenetic processes that led to their formation. However, the intense hydrothermal alteration associated with porphyry copper deposits prevents the assessment of the petrogenetic processes controlling the magma fertility using classical whole rock geochemistry.

Yet, apatite geochemistry has recently been used to assess metallogenetic fertility of different mineral deposits at a regional scale as well as the role of the magmatic processes involved in their formation (e.g., Belousova et al., 2001; Belousova et al., 2002; Cao et al., 2012; Mao et al., 2016). Apatite incorporates geologically valuable elements that are sensitive to the evolution of magmas, such as rare-earth elements (REE), Sr, Y, Th and U (e.g., Sha and Chappell, 1999; Piccoli and Candela, 2002; Prowatke and Klemme, 2006; Bruand et al., 2017). Also, it has recently been proposed as a porphyry indicator mineral (PIMS) because it records magmatic and hydrothermal processes associated with the formation of porphyry copper deposits (e.g., Loader, 2017; Bouzari et al., 2017).

This study aims to characterize the chronology and the petrogenetic processes responsible for the generation of the ore-poor and ore-rich porphyritic bodies associated with Cu-Mo mineralization in the Buenavista del Cobre deposit. To this end, we dated the crystallization ages of the porphyry intrusions related to the different magmatic events that generated the mineralization. In addition, we used apatite trace element compositions as a proxy to identify the petrogenetic processes involved in the formation of ore-rich and ore-poor porphyry intrusions and to evaluate the role of the oxidation state and volatile content of these magmas in the mineralization process.

2. Geological background

2.1. Regional geological setting

The Cananea Mining District consists of several porphyry copper deposits, including El Pilar, Milpillas, Lucy, Mariquita, María, Buenavista del Cobre Cu-Mo deposits and the El Alacrán prospect (Fig. 1). The basement of the District is represented by the Precambrian Cananea anorogenic Granite (1.44 Ga; Anderson and Silver, 1977; Fig. 1) that intruded the Precambrian metamorphic rocks of the Mazatzal province (Anderson and Silver, 1981; Eisele and Isachsen, 2001; Whitmeyer and Karlstrom, 2007). In the Cananea Mining District, Paleozoic sedimentary rocks associated with the passive margin of Laurentia in southwestern North America (Stewart, 1988) are represented by quartzite and limestone that unconformably overlie the Cananea Granite (Meinert, 1982; Fig. 1). During the Triassic-Jurassic, a Cordilleran magmatic arc developed in Arizona and Sonora (Gastil et al., 1978; Tosdal et al., 1989) associated with the subduction of the Kula plate beneath the North American Plate (Brass et al., 1983). This Jurassic arc lead to the formation of volcanic and plutonic rocks ranging in age from 180 to 150 Ma (Coney and Reynolds, 1977; Anderson et al., 2005; Rodríguez-Castañeda and Anderson, 2011; Valencia-Moreno et al., 2023). In the Cananea Mining District, Meinert (1980) suggested that this period of magmatism is probably represented by the Elenita and Henrietta volcanic Formations (Valentine, 1936; Fig. 1) and the El Torre Syenite pluton (Emmons, 1910; Fig. 1). The Elenita Formation is composed by a sequence of rhyolitic to andesitic tuff and flows with interbedded sandstone and quartzite (Valentine, 1936). The Henrietta Formation is composed by medium- to high-K, calc-alkaline, dacitic to rhyolitic tuff (Wodzicki, 1995) and contains clasts of rocks from the Elenita Formation (Valentine, 1936). The El Torre Syenite was described by Valentine (1936) as a pinkish-gray rock mainly composed of feldspar and hornblende ± biotite ± quartz and other accessory minerals.

After a magmatic activity hiatus during the Early Cretaceous, subduction-related arc magmatism was reactivated at the end of the Early Cretaceous, associated with the subduction of the Kula-Farallon oceanic plates beneath the southwestern North American plate (Coney and Reynolds, 1977). During the Late Cretaceous-Paleogene, a northeastward migration of the arc magmatism associated with a change in the subduction angle was documented in southwestern North America (Coney and Reynolds, 1977; Engebretson et al., 1985; Stock and Molnar, 1988). In Sonora, this period of magmatic activity has been historically referred to as the "Laramide magmatic arc" because it was contemporaneous of the Laramide orogeny (e.g., McDowell et al., 2001). However, Valencia-Moreno et al. (2021) suggested that this term should be changed to "Cretaceous-Eocene Mexican Magmatic Arc" (CEMMA) due to the characteristics of this arc in terms of tectonic style and magmatism. It is during this period of magmatism, that the porphyry copper deposits of the Arizona-Sonora-New Mexico cluster were emplaced (Valencia-Moreno et al., 2016; Fig. 1).

In the Cananea Mining District, Late Cretaceous volcanic rocks associated with the CEMMA are represented by the Mariquita and Mesa Formations (Valentine, 1936; Fig. 1). The latter has been dated between ~ 72.6 and ~ 65.8 Ma by the $^{40}Ar/^{39}Ar$ method (Wodzicki, 1995; Cox et al., 2006). The Tinaja Diorite and the Cuitaca Granodiorite represent the plutonic part of this magmatic arc (Valentine, 1936; Meinert, 1982; Wodzicki, 1995; Fig. 1). Both plutons share geochemical similarities and form a composite batholith called the Tinaja-Cuitaca Batholith (Valentine, 1936; Wodzicki, 1995; Fig. 1). Zircon U-Pb ages of 64 ± 3 Ma and 63.8 ± 1.1 Ma were obtained for the Cuitaca Granodiorite (Anderson and Silver, 1977; Del Rio-Salas et al., 2013). At the end of the emplacement of the Tinaja-Cuitaca Batholith, a series of quartz-feldspathic porphyry intrusions (closely related with several breccia pipes and important copper-molybdenum mineralization) emplaced between ~ 64 and ~ 57 Ma (Meinert, 1982; Bushnell, 1988; Valencia et al., 2006; Del Rio-Salas et al., 2013 and 2017; Fig. 1).

After the Late Cretaceous-Early Paleogene magmatism, Sonora experienced a period of tectonic quiescence from the Paleocene to the Oligocene (Wong et al., 2010). This was followed by a period of intense magmatism associated with the ignimbrite "flare-up" that culminated with the formation of the Sierra Madre Occidental during the Oligocene (Ferrari et al., 2018). After this period, the Basin and Range continental extension began, interpreted as a consequence of slab rollback or post-orogenic collapse of the crust (Coney and Harms, 1984; Wernicke, 1992; Sonder and Jones, 1999). In Sonora, this extension was active from the Oligocene to the early Miocene (Nourse et al., 1994; McDowell et al., 1997; Gans, 1997; Vega-Granillo and Calmus, 2003; Wong and Gans, 2003; Wong et al., 2010). In the Cananea Mining District, the extension triggered the development of N-S trending normal faults (Wodzicki, 2001; Fig. 1). It resulted in a regional eastward tilting of the Mesa Formation and several breccia pipes (Perry, 1961; Meinert, 1982; Bushnell, 1988; Fig. 1) across the district, as well as the formation of continental basins filled by clastic deposits intercalated with basaltic flows of Oligo-Miocene age (Fig. 1).

2.2. Geology of Buenavista del Cobre deposit

The Buenavista del Cobre deposit is located in a tilted block controlled to the west by a west-dipping normal fault (Fig. 1 and 2). This deposit is a typical porphyry Cu-Mo deposit where hypogene mineralization is found within porphyry intrusions, high-grade breccia pipes, as disseminated sulfides, as well as in stockwork veinlets (Perry, 1935 and 1961; Meinert, 1980; Bushnell, 1988; Virtue, 1996). Post-mineralization exhumation associated with Basin and Range extension promoted the development of a thick (up to 500 m) supergene chalcocite blanket where the current mining activity is focused (Virtue, 1996; Ayala-Fontes, 2009).

In the Buenavista del Cobre deposit, the Proterozoic Cananea Granite is a coarse-grained plutonic rock that consists of centimetric K-feldspar, subhedral plagioclase and sub-rounded quartz crystals (Fig. 3A). It is unconformably overlain by the Paleozoic sediments in the northern part

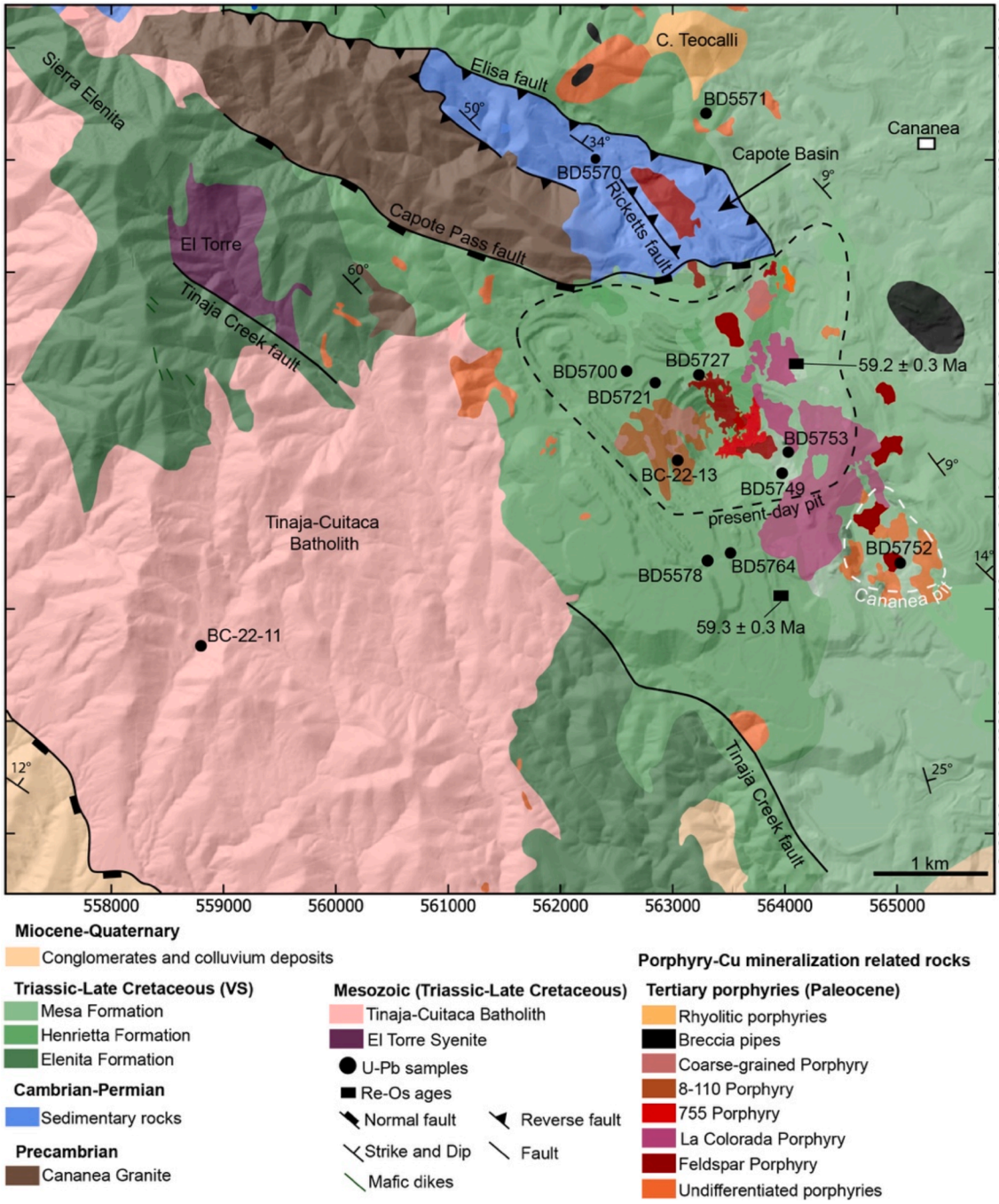

Fig. 2. Geological map of the Buenavista del Cobre porphyry copper deposit, modified from Meinert (1982), Wodzicki (1995), Noguez-Alcántara (2008), Ortiz-Olvera (2022), and the geological department of Buenavista del Cobre mine. VS: volcano-sedimentary rocks.

of the deposit (Fig. 2). This area corresponds to a horst-like structure bounded by the WNW-ESE trending Elisa and Capote Pass faults (Emmons, 1910; Valentine, 1936; Meinert, 1980; Ortiz-Olvera, 2022; Fig. 2). There, the Paleozoic sedimentary rocks of the Bolsa, Abrigo, Escabrosa and Martin Formations, and the Naco Group developed Zn-Cu skarn mineralization (Meinert, 1980). The oldest volcanic rocks correspond to the Elenita and Henrietta Formations which crop out in the western and central part of the area, respectively (Fig. 2). The Henrietta Formation is considered to be younger than the Elenita Formation (Valentine, 1936). The Elenita Formation was intruded by the El Torre Syenite which is cut by the NW-SE trending Tinaja Creek fault at Sierra Elenita (Valentine, 1936; Fig. 2). The Henrietta and Elenita Formations are in a structural contact south of the deposit along the Tinaja Creek fault, which is supposed to be normal (Fig. 2). The Mesa Formation is mainly exposed in the central and eastern areas of the deposit where it gently dips (~15°) to the east (Fig. 2). The intrusive rocks of Tinaja-Cuitaca Batholith crop out to the northwest and to the west of the current mine operation (Fig. 2).

A series of ore-related porphyries intruded and hydrothermally altered and mineralized the entire rock section mentioned above (Ochoa-Landín and Echávarri-Pérez, 1978; Perry, 1935; Valentine, 1936; Ochoa-Landín and Navarro-Mayer, 1979; Meinert, 1980; Bushnell, 1988; Wodzicki, 1995; Fig. 2). The relative age of these intrusions has been established based on crosscutting-relationships (Ochoa-Landín and Echávarri-Pérez, 1978; Ochoa-Landín and Navarro-Mayer, 1979).

The ore-poor Feldspar Porphyry was the first emplaced in the area

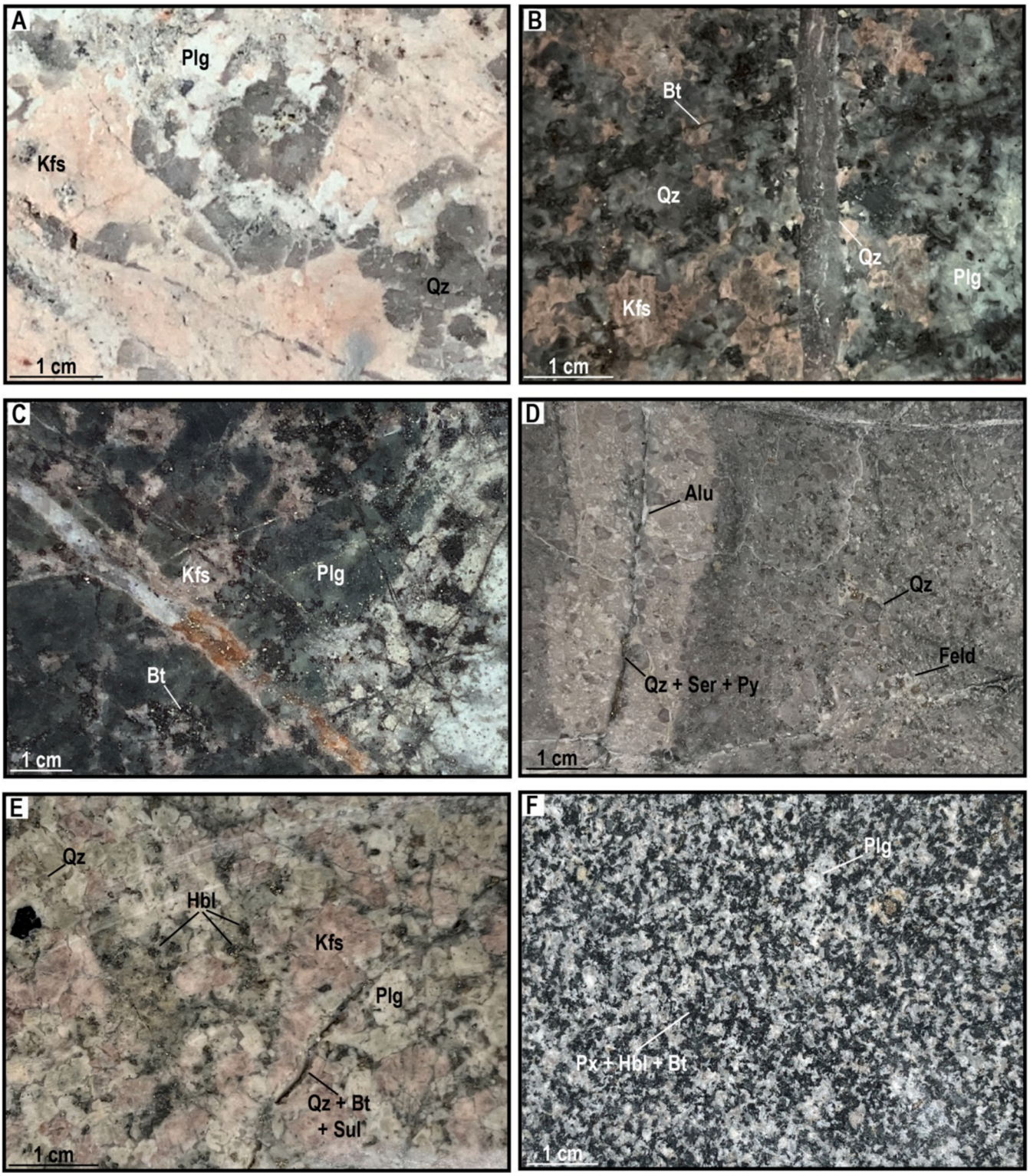

Fig. 3. Hand specimens of mineralized host rocks dated in this study. A) Cananea Granite (sample BD5753-468 m). Note the selective alteration of plagioclase to sericite. B) Plutonic rock (sample BD5752-669 m) with a coarse-grained texture of K-feldspar, plagioclase, quartz, and biotite. C) Coarse-grained plutonic rock (sample BD5753-627 m) composed by K-feldspar, plagioclase, quartz and biotite. D) Volcanic flow of the Henrietta Formation (sample BD5571-180 m) showing a porphyritic texture of anhedral quartz and feldspar phenocrysts embedded in a quartz-sericite groundmass. E) Medium-grained plutonic rock (sample BD5578-690 m) composed mainly of K-feldspar, plagioclase with minor quartz, hornblende, and biotite. F) Tinaja Diorite (sample BC-22–11) showing a phaneritic texture composed mainly of plagioclase (>90 %) with minor quartz, pyroxene, hornblende, and biotite. Qz = quartz; Feld = feldspars; Kfs = potassic feldspar; Plg = plagioclase; Px = pyroxene; Hbl = hornblende; Bt = biotite; Ser = sericite; Sul = sulfides; Alu = alunite. The same abbreviations will be used henceforth.

and crops out in the center of the present open pit and in the Capote Basin (Fig. 2), where it was emplaced along NW-SE trending fractures (Ochoa-Landín and Navarro-Mayer, 1979; Fig. 2). It is a quartz-monzodioritic porphyry composed of 1–2 mm feldspar phenocrysts, and 1 mm anhedral quartz crystals embedded in a fine matrix of quartz-sericite (Fig. 4A). Feldspars show chloritic alteration overprinted by sericitic alteration. Some biotites are brown to colorless due to the sericitization. Sulfides are associated with disseminated sericite, replacing mafic minerals, and occur in quartz veinlets with sericitic envelopes (Fig. 4A). According to Ochoa-Landín and Navarro-Mayer (1979), this ore-poor intrusion was followed by the subsequent emplacement of the La Colorada, 755 and 8–110 porphyries along N-S fractures or faults (Fig. 2).

The ore-rich La Colorada Porphyry crops out in the eastern part of the present-day pit (Fig. 2) and is composed by 2–7 mm subhedral feldspar phenocrysts, and 2–3 mm sub-rounded quartz crystals and biotite phenocrysts in a quartz and feldspar fine-grained matrix. Feldspars from the La Colorada Porphyry show a strong silicification and thin K-feldspar veinlets (Fig. 4B). The high-grade La Colorada breccia pipe is genetically and spatially related to the La Colorada Porphyry as it occurs at its top, where it mimics the shape of the stock (Perry, 1935 and 1961; Bushnell, 1988). The breccia pipe is a high-grade orebody characterized by pegmatitic silicate-sulfide mineralization (6 Mt, 7 % Cu and 0.8 % Mo; Perry, 1935 and 1961; Wodzicki, 1995). Today, this breccia no longer exists as it has been completely mined. The age of the mineralization at the top of this breccia has been constrained to 59.2 ± 0.3 Ma (molybdenite Re-Os dating; Barra et al., 2005; Fig. 2).

The ore-rich 755 Porphyry is located in the central part of the open pit, where it crosscuts the Feldspar Porphyry (Fig. 2). This intrusive consists of feldspars phenocryst and 2–3 mm quartz crystals embedded in a fine silicified matrix of quartz and feldspars.

The ore-poor 8–110 Porphyry crops out in the western part of the present-day pit (Fig. 2). It only intrudes the Henrietta Formation. It is composed by 2–7 mm feldspar and 1 mm quartz phenocrysts with biotite and hornblende embedded in a fine matrix composed by quartz, feldspars and sericite (Fig. 4C). In this rock, felspars are altered to chlorite and later to sericite. Hornblende has a fibrous texture and green color because of biotitization. Early thin K-feldspar veinlets and late quartz-sericite-pyrite veins crosscut the porphyry (Fig. 4C). Sulfides occur in disseminations and are associated with coarse-grained sericite crystals. A low Cu grade tourmaline breccia is spatially related to this porphyry stock (Varela, 1972).

The ore-poor Coarse-grained Porphyry is often considered as the last intrusion emplaced in the deposit. This porphyritic body crosscuts the 8–110 Porphyry in the western part of the present-day pit (Fig. 2). It is composed of < 7 mm plagioclase phenocrysts, <20 mm K-feldspar (orthoclase) phenocrysts, and < 5 mm sub-rounded quartz crystals (Fig. 4D). In this rock, sulfides occur as disseminated pyrite crystals.

In this study, we report a newly discovered ore-rich porphyry (here referred to as the El Galo Porphyry, Fig. 4E and F). This porphyry does not crop out at the current level of mining and was identified in the drill hole BD5764 south of the present-day open pit (Fig. 2). In that area, it intrudes the volcanic rocks of the Henrietta Formation (Fig. 2). It is composed by K-feldspar, plagioclase, minor quartz, biotite and hornblende phenocrysts embedded in a fine matrix of quartz + feldspar + biotite (Fig. 4E). In this rock, feldspars were altered by early chlorite and later by sericite, and hornblende was completely replaced by small flakes of biotite. The emplacement of this porphyry was accompanied by an important potassic alteration characterized by the development of biotite + quartz + chalcopyrite + molybdenite + pyrite + anhydrite veins (Fig. 4F).

Additionally, a set of sericitically altered and barren porphyry stocks consisting of large rhyolitic plugs crop out north of the Buenavista del Cobre deposit (Wodzicki, 2001; Fig. 2). At Cerro Teocalli, the sericite alteration has been dated in a rhyolitic porphyry at 54.2 ± 2 Ma (K-Ar on sericite; Wodzicki, 1995).

2.2.1. Alteration and mineralization

The alteration and mineralization patterns at Buenavista del Cobre deposit are complex. Mineralization occurs in disseminated deposits with stockwork veinlets, breccia pipes, breccia zones and skarn deposits (Meinert, 1980; Bushnell, 1988; Wodzicki, 1995; Virtue, 1996). For practical purposes, the alteration and mineralization processes associated with Cu-Mo mineralization has been divided into early and late alteration and mineralization, based on cross-cutting relationships (Bushnell, 1988). The alteration and mineralization related to the development of skarn deposits is beyond the scope of this study, but the reader is referred to Meinert (1980) for a detailed description.

Early alteration and the precipitation of disseminated sulfides have been interpreted as being associated with the emplacement of the La Colorada Porphyry and formation of the La Colorada breccia pipe (Bushnell, 1988 and references therein). This alteration consists of thin veinlets of quartz, K-feldspar and sulfides in conjunction with metasomatic K-feldspar and biotite (Bushnell, 1988). At La Colorada breccia pipe, a potassic alteration consisting of quartz + K-feldspar + biotite pegmatitic zones with Cu(Fe) sulfides, and molybdenite has been described (Wodzicki, 1995). The age of this alteration was constrained by K/Ar on phlogopite at 59.9 ± 2.1 Ma (Damon and Mauger, 1966) and 58.5 ± 2.1 Ma (Varela, 1972). Moreover, widespread propylitic alteration characterized by partial replacement of ferromagnesian minerals by actinolite and chlorite ± sphene ± rutile, and alteration of plagioclase to sericite ± clays and epidote is probably contemporaneous with the early mineralization (Virtue, 1996; Wodzicki, 1995). This propylitic alteration is well developed at the Tinaja and El Torre plutons, to the west of the study area (Wodzicki, 1995).

Late alteration has been interpreted to correspond to quartz-sericite (phyllic) hydrothermal alteration. This alteration type is the dominant alteration at the Buenavista del Cobre deposit and extends to a depth of ~ 1 km (Schwartz, 1947; Meinert, 1980; Bushnell, 1988; Virtue, 1996). At shallow levels, this alteration overprints the early alteration mineral assemblages described above. The associated hypogene mineralization occurs mainly disseminated within the volcanic host rocks and within the porphyries, and has been dated by Re-Os on molybdenite at 59.3 ± 0.3 Ma in a phyllic-altered quartz-feldspar porphyry with disseminated chalcopyrite and molybdenite (Barra et al., 2005). The intense and pervasive phyllic alteration is characterized by the replacement of feldspars by sericite and of the mafic minerals by sericite ± pyrite ± chalcopyrite (Wodzicki, 1995).

A late argillic alteration is also reported at the Buenavista del Cobre deposit. It consists of fine-grained clay (kaolinite), quartz, and alunite (Wodzicki, 1995; Virtue, 1996). It was locally documented in the upper levels of La Colorada Porphyry where the sericitic alteration is crosscut by alunite veinlets (Perry, 1961; Wodzicki, 1995), and in some areas of the disseminated mineralization. An hypogene origin for this alteration has been proposed (Wodzicki, 1995; Bushnell, 1988). However, host rock interaction with supergene acid fluids may be the origin of some argillic alteration zones and alunite veinlets (Bushnell, 1988; Virtue, 1996).

A thick supergene alteration profile characterizes the Buenavista del Cobre deposit and makes it economically significant. It consists, from top to bottom, of a leached capping oxide zone, a secondary copper sulfide enriched zone, a partially enriched zone (mixture of hypogene and supergene mineralization), and a primary mineralization zone (Virtue, 1996). The supergene enrichment mineralogy mainly consists of chalcocite and covellite replacing and coating hypogene Cu sulfides in disseminations and veinlets (Virtue, 1996).

2.2.2. Structure

Several major faulting episodes have been reported in the Buenavista del Cobre deposit. An early episode is represented by a group of steeply dipping WNW-ESE trending faults corresponding to the Elisa, Capote Pass, Tinaja Creek, and Ricketts faults (Emmons, 1910; Valentine, 1936; Fig. 2). In particular, the Elisa and Capote Pass faults bound the Cananea

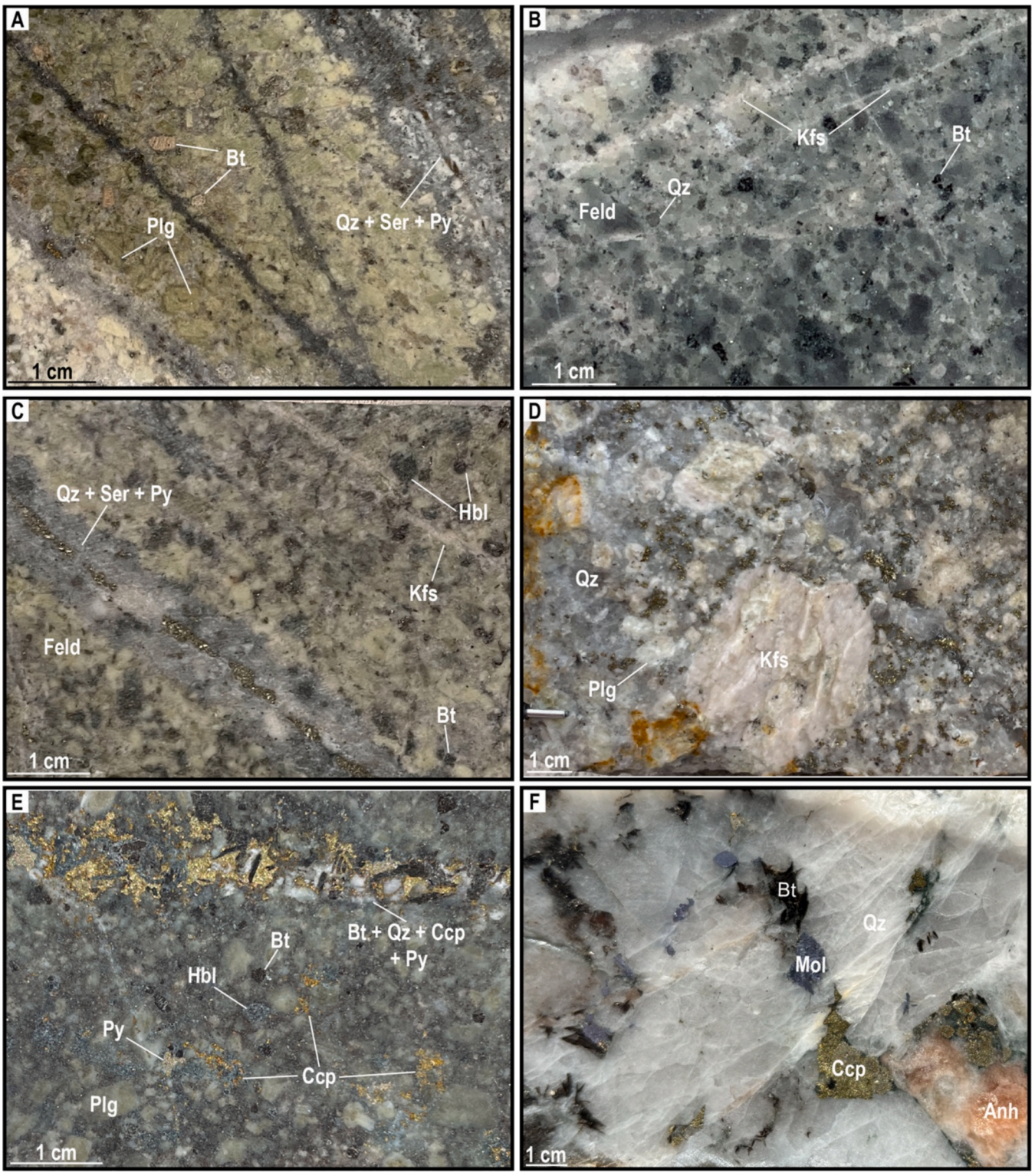

Fig. 4. Hand specimens of main porphyries dated in this study. A) Feldspar Porphyry (sample BD5570-613 m) showing a porphyritic texture composed of feldspars with minor quartz and biotite embedded in a fine matrix of quartz + sericite. B) La Colorada Porphyry (sample BD5753-815 m) showing feldspar, quartz, and biotite phenocrysts embedded in a fine matrix of quartz and feldspar. The 755 Porphyry presents a similar texture and mineralogy. C) 8–110 Porphyry (sample BD5721-574 m) showing a coarse-grained texture composed of feldspar phenocryst with quartz, biotite and hornblende. Note the quartz-sericite-pyrite veins and the thin K-feldspar veinlets. D) Coarse-grained Porphyry (sample BC-22–13) composed by quartz + K-feldspar + plagioclase. Sulfides correspond to disseminated pyrite crystals. E) El Galo Porphyry (sample BD5764-826 m) mineralogy consists of feldspar, minor quartz, and biotite and hornblende phenocrysts. Note the chalcopyrite disseminations and the biotite + quartz + sulfides vein that crosscuts the porphyry. F) Potassic alteration associated with the El Galo Porphyry emplacement showing a coarse-grained quartz-biotite vein associated with the precipitation of chalcopyrite, molybdenite, pyrite and anhydrite. Py = pyrite; Ccp = chalcopyrite; Mol = molybdenite; Anh = anhydrite.

Granite and the Paleozoic sedimentary rocks in the Capote Basin (Fig. 2). The NNW-SSE Ricketts reverse fault cuts part of the Paleozoic sequence (Ortiz-Olvera, 2022; Fig. 2). The Tinaja Creek fault controls the southwestern border of the El Torre Syenite pluton and separates the Elenita Formation from the Henrietta Formation in the western part of the deposit (Fig. 2). The interpretation of the kinematics of these faults remains poorly documented. Ortiz-Olvera (2022) proposed that the Elisa and Ricketts faults are reverse faults that were active between 67 and 64 Ma during the Laramide compression. In addition, a normal displacement sense of faulting has been proposed for the Capote Pass fault, which was probably active in the Oligo-Miocene during the Basin and Range extension (Ortiz-Olvera, 2022).

A late episode of faulting is represented by N-S to NW-SE trending normal faults that cut all the rocks in the deposit. In particular, the main faults belonging to this family occur at the westernmost border of the study area (Fig. 2) and control the tilting of the structural block where the deposit occurs. This post-mineralization faulting consists of high-angle normal faults associated with the Basin and Range extension and influenced the oxidation and supergene enrichment in the Buenavista del Cobre deposit (Bushnell, 1988; Wodzicki, 1995; Virtue, 1996).

3. Methodology and analytical techniques

Samples of texturally and compositionally different porphyritic and intrusive host rocks were taken either from drill holes or outcrops at different locations in the Buenavista del Cobre deposit (Fig. 2). A complete petrographic description of the analyzed samples can be found in the Supplementary material (S1). Four samples from the igneous host rocks (Fig. 2 and 3), one sample from the precursor batholith (Tinaja Diorite; Fig. 2 and 3F) and five different samples from the main porphyry intrusions were collected for zircon U-Pb geochronology (Fig. 2 and 4). Concerning apatite trace elements compositions and U-Pb geochronology, two samples from the igneous host rocks and six samples from ore-related porphyries were analyzed. In order to compare the apatite geochemical characteristics of the ore-rich and ore-poor porphyry intrusions at Buenavista del Cobre deposit, the main porphyries (Fig. 4) were sampled based on their metal contribution and were divided into two groups: (1) ore-rich porphyries represented by La Colorada, 755 and El Galo porphyries samples, and (2) ore-poor porphyries represented by the 8–110 and the Coarse-grained porphyries samples.

After crushing and sieving, magnetic and heavy mineral separation techniques were used to isolate zircon and apatite crystals. Crystals were then hand-picked from the heavy fraction under a binocular microscope. Around 50–100 apatite and zircon grains for each sample were embedded in an epoxy resin and polished to expose their inner part.

LA-ICP-MS U-Pb dating was performed on all the collected samples. All analyses were performed at the GeOHeLiS Plateform, University of Rennes, France, using an ESI NWR193UC Excimer laser coupled to an Agilent 7700x Q-ICP-MS. The analytical procedure and instrument operating conditions are detailed in the Supplementary file S2. Zircon grains were imaged by cathodoluminescence and then analyzed with a 25 μm round spot (Supplementary material S3), with a repetition rate of 4 Hz and a fluence of 6 J/cm^2. The GJ-1 zircon was used as a primary standard (Jackson et al., 2004), while the Plesovice (Sláma et al., 2008) and Fish Canyon Tuff (Boehnke and Harrison, 2014) zircon reference materials were used for quality control. Additional information on the analytical protocol can be found in Nosenzo et al. (2022). Apatite U-Pb and trace elements concentration data were acquired using apatite fission track protocol of Cogné et al. (2020) on inclusion free-grains, using a 30 μm round spot with a 5 Hz repetition rate and a 4 J/cm^2 fluence. For U-Pb standard bracketing, the Madagascar apatite (Thomson et al., 2012) was used as a primary standard, the McClure apatite (Schoene and Bowring, 2006) and Durango apatite (McDowell et al., 2005) were employed as quality control material.

Data reduction was carried out with the Iolite data reduction scheme U–Pb Geochronology (Paton et al., 2011) for zircon, and the data reduction scheme Vizual-Age_UcomPbine (Chew et al., 2014a) for apatite. Concordia ages and diagrams were generated using IsoplotR (Vermeesch, 2018). In the case of zircon U-Pb data, a threshold of ± 2 % of concordance of a single grain was used to select zircon grains for concordia date calculations. Concordia dates are quoted with two uncertainties, without and with systematic uncertainties propagated (Horstwood et al., 2016; Table 1).

Apatite Cl (wt %) concentrations were calculated using the protocol of Chew et al. (2014b) with McClure apatite as a low-Cl standard and a synthetic Cl-apatite (Klemme et al., 2013) as a high-Cl standard. Trace element data were reduced using the TraceElement DRS, with NIST 612 as external standard (Jochum et al., 2011) and ^{43}Ca as internal standard with a value 39.36 % for apatite. McClure apatite are used as quality control material (Cogné et al., 2024). Concentration calculated were then normalised to chondrite values (Barrat et al., 2012). Eu and Ce anomalies were calculated according to Lodders (2010) with Eu/Eu* =

Table 1
Zircon and apatite U-Pb dates for the Buenavista del Cobre host rocks and main porphyries. Coordinates in WGS84, UTM zone 12.

Sample ID	Rock type	Coordinates		Elevation (m)	U-Pb date (Ma)
		UTM (N)	UTM (E)		
Zircon U-Pb dating					
BD5753-468 *m*	Intrusive host rock	3,425,398	564,031	1107	**1421 ± 14/18**
BD5752-669 *m*	Intrusive host rock	3,424,409	565,029	889	**186.9 ± 1.3/3.1**
BD5571-180 *m*	Henrietta Formation	3,428,416	563,299	1594	**186.8 ± 1.1/3.0**
BD5578-690 *m*	Intrusive host rock	3,424,429	563,312	1094	**176.3 ± 1.1/2.9**
BC-22–11	Tinaja Diorite	3,423,671	558,799	1704	**73.8 ± 0.6/1.3**
BD5570-613 *m*	Feldspar Porphyry	3,428,010	562,314	1175	**59.7 ± 0.5/1.1**
BD5753-815 *m*	La Colorada Porphyry	3,425,398	564,031	760	**58.9 ± 0.5/1.0**
BD5749-606 *m*	755 Porphyry	3,425,209	563,977	969	**57.5 ± 0.2/0.9**
BD5721-574 *m*	8–110 Porphyry	3,426,015	562,846	895	**56.5 ± 0.3/0.9**
BD5764-826 *m*	El Galo Porphyry	3,424,498	563,516	948	**56.1 ± 0.2/0.9**
Apatite U-Pb dating					
BD5753-627 *m*	Intrusive host rock	3,425,398	564,031	948	**56.7 ± 4.6**
BD5578-690 *m*	Intrusive host rock	3,424,429	563,312	1094	**54 ± 10**
BD5753-815 *m*	La Colorada Porphyry	3,425,398	564,031	760	**59.2 ± 2.2**
BD5749-606 *m*	755 Porphyry	3,425,209	563,977	969	**58.3 ± 3.1**
BD5727-547 *m*	8–110 Porphyry	3,426,084	563,237	833	**56.8 ± 2.6**
BD5700-711 *m*	8–110 Porphyry	3,426,116	562,591	827	**56.8 ± 1.9**
BD5721-574 *m*	8–110 Porphyry	3,426,015	562,846	895	**56.0 ± 4.6**
BD5764-826 *m*	El Galo Porphyry	3,424,498	563,516	948	**57.0 ± 8.2**

$Eu_{CN} \bullet (Sm_{CN} \bullet Gd_{CN})^{-0.5}$ and $Ce/Ce^* = Ce_{CN} \bullet (La_{CN} \bullet Pr_{CN})^{-0.5}$.

4. Results

4.1. Petrology of the El Galo Porphyry

In this study, we report a newly discovered porphyry (here referred as El Galo Porphyry) intersected by exploration drilling. This porphyry does not crop out at the current level of mining and was identified in the drill hole BD5764 to the south of the present-day open pit where it intrudes and mineralizes the volcanic rocks of the Henrietta Formation (Fig. 2). It is composed by K-feldspar, plagioclase, minor quartz, biotite and hornblende phenocrysts embedded in a fine matrix of quartz + feldspar + biotite (Fig. 4E). This porphyry is spatially associated with a potassic alteration zone expressed as massive coarse-grained hydrothermal veinlets of biotite + quartz + chalcopyrite + pyrite + molybdenite + anhydrite, and disseminations of chalcopyrite, molybdenite and pyrite (Fig. 4F). Based on these observations, we classify the El Galo Porphyry as an ore-rich porphyry such as the La Colorada and 755 porphyries.

4.2. Zircon U-Pb dating

Four new zircon U-Pb dates (Table 1) have been obtained from different igneous host rocks at Buenavista del Cobre deposit (Wetherill and Tera-Wasserburg concordia plots are reported in Figure 5 and data in Supplementary Table S4). Zircon grains from sample BD5753-468 m, supposedly belonging to the Cananea Granite (Fig. 3A), are predominantly prismatic and elongated (186–350 μm in size) and show oscillatory or patchy zoning (e.g., G15 and G13, respectively; S3 Fig. 1). The analyzed zircon grains show high U (186–2525 ppm) and Pb (330–1012 ppm) contents with Th/U ratios ranging from 0.11 to 0.31. Thirty analyses performed in zircon rims (S3 Fig. 1) define a discordia line with an upper intercept date of 1421 ± 14/18 Ma and a lower intercept date of

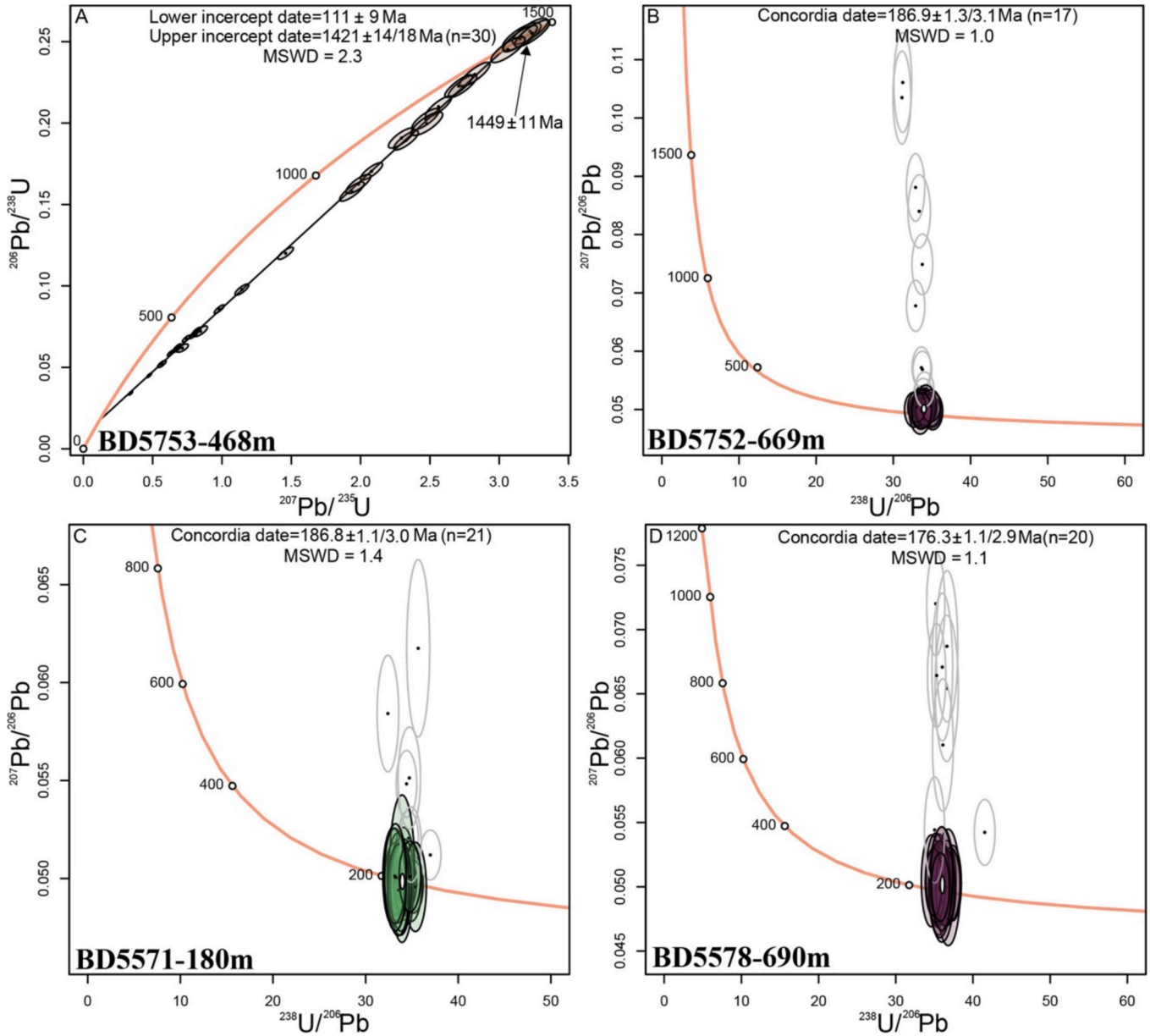

Fig. 5. Wetherill and Tera-Wasserburg concordia plots of zircon U-Pb analysis of the intrusive host rocks of the Buenavista del Cobre deposit. Concordia dates are reported with two different uncertainties separated by a dash bar (/): the first one without propagating the systematic uncertainties and the second after proper propagation (Horstwood et al., 2016).

111 ± 9/9 Ma (n = 30, MSWD = 2.3; Fig. 5A). Five analyzed zircon grains yield a concordia date of 1449 ± 11 Ma (n = 5, MSWD = 1.1; Fig. 5A).

We also analyzed zircons from sample BD5752-669 m, a coarse-grained intrusive host rock with K-feldspar, plagioclase, quartz and biotite phenocrysts (Fig. 3B). In this rock, plagioclase is altered to chlorite and mafic minerals are replaced by small grains of biotite. Thin veinlets of biotite crosscut the rock and are cut by late quartz-sericite veins. Sulfides are associated with biotite and quartz-sericite veins, and also occur as disseminations. Zircon crystals from this rock are stubby, euhedral to subhedral (166 to 373 μm in size), mostly with a concentric oscillatory zoning (S3 Fig. 1) and less commonly with patchy zoning (e.g., G23; S3 Fig. 1). They can also present inherited cores (e.g., G22; S3 Fig. 1). All the analyses were performed in the zircon rims (S3 Fig. 1) and show variable U (310–1248 ppm) and Pb (65–2086 ppm) contents with Th/U ratios ranging from 0.23 to 0.34. Seventeen zircon analyses yield a concordia date of 186.9 ± 1.3/3.1 Ma (n = 17, MSWD = 1.0; Fig. 5B). The remaining analyses are discordant because of the presence of a non-negligible and variable amount of common Pb (f206c > 0.2 %, Supplementary Table S4).

Sample BD5571-180 m corresponds to a porphyritic volcanic rock of the Henrietta Formation conformed by anhedral quartz and feldspar phenocrysts embedded in a quartz-sericite groundmass (Fig. 3D). Quartz-pyrite veinlets with sericite envelopes are common in this sample of the Henrietta Formation, it has to be noted that thin supergene white alunite veinlets tapped the quartz-sericite veinlets to precipitate. Zircons from this sample are prismatic (240–333 μm in size) with concentric oscillatory zoning and, more rarely, patchy zoning (e.g., G24; S3 Fig. 1). All the analyses were performed in the zircon rims (S3 Fig. 1). They show high U (278–4850 ppm) and Pb (57–1828 ppm) contents with Th/U ratios ranging from 0.18 to 0.83. Twenty-one zircon analyses yield a concordia date of 186.8 ± 1.1/3.0 Ma (n = 21, MSWD = 1.4; Fig. 5C). The remaining data are discordant due to the presence of common Pb in the crystals lattice (f206c > 0.2 %, Supplementary Table S4).

Finally, sample BD5578-690 m corresponds to a medium-grained plutonic host rock composed of K-feldspar and plagioclase with minor quartz, hornblende and biotite (Fig. 3E). In this rock, hornblende is often replaced by small grains of biotite, and selective chloritization of plagioclase is observed. Thin veinlets of quartz + biotite + sulfides crosscut the rock (Fig. 3E). Zircon crystals from this sample are prismatic (166–369 μm in size) with oscillatory (e.g., G5; S3 Fig. 1) and patchy zoning (e.g., G26, G7 and G10; S3 Fig. 1). They can sometimes display some inherited cores (e.g., G23; S3 Fig. 1). Zircon grains have low U (30–121 ppm) and Pb (18–225 ppm) contents with Th/U ratios ranging from 0.20 to 0.33. Twenty analyses performed in the zircon rims (S3 Fig. 1) yield a concordia date of 176.3 ± 1.1/2.9 Ma (n = 20, MSWD = 1.1; Fig. 5D). Here again, the remaining data are discordant because of the presence of a non-negligible amount of common Pb (f206c > 0.6 %, Supplementary Table S4).

Six new zircon U-Pb dates (Table 1) are reported for the precursor batholith and ore-related porphyry rocks (Tera-Wasserburg concordia plots are reported in Figure 6 and data in Supplementary Table S4). Zircon grains from the Tinaja Diorite (sample BC-22–11; Fig. 2) are stubby, euhedral to subhedral (266–340 μm in size) with distinct morphology and texture when compared to the zircon crystals from the porphyry rocks (S3 Fig. 2). Indeed, the crystals commonly exhibit a zoning marked by wide dark-CL zones and narrow bright-CL zones (S3 Fig. 2) and, less commonly, are characterized by the presence of concentric oscillatory (eg., G5; S3 Fig. 2) or patchy zoning (G7; S3 Fig. 2). All the analyses were performed in zircon outer parts (S3 Fig. 2) and show variable U (445–2448 ppm) and Pb (34–372 ppm) contents with Th/U ratios ranging from 0.13 to 0.50. Twenty-three U-Pb zircon analyses yield a concordia date of 73.8 ± 0.6/1.3 Ma (n = 23, MSWD = 2.0; Fig. 6A). The remaining analyses plot in a discordant position owing for the presence of a non-negligible amount of common Pb (f206c up to 18 %, Supplementary Table S4).

Five zircon U-Pb dates have been obtained from the main porphyritic intrusions at Buenavista del Cobre deposit (Table 1; Fig. 6), which are compositionally and texturally different (Fig. 4). In general, zircon grains from porphyry rocks have needle-like shapes (80–380 μm in size) with concentric oscillatory growth zoning (S3 Fig. 2), which is typical of magmatic zircon that crystallized in fast-cooling intrusions (Corfu et al., 2003; Nathwani et al., 2023). Zircon grains from sample BD5570-613 m collected from the NW-SE trending Feldspar Porphyry (Fig. 2) show variable U (510–1824 ppm) and Pb (35–333 ppm) contents with Th/U ratios ranging from 0.23 to 0.71. Fifteen zircon U-Pb analyses performed either in the inner or the outer parts of the grains (S3 Fig. 2) yield a concordia date of 59.7 ± 0.5/1.1 Ma (n = 15, MSWD = 0.4; Fig. 6B). A second group of four concordant analyses yield a concordia date of 65.1 ± 1.0/1.5 Ma (n = 4, MSWD = 0.4; Fig. 6B), while one grain is concordant at ca. 174 Ma (Fig. 6B). The remaining data are discordant due to the presence of common Pb (f206c > 0.4 %, Supplementary Table S4).

Zircon crystals from the La Colorada Porphyry (sample BD5753-815 m) show variable U (175–1132 ppm) and Pb (13–329 ppm) contents and Th/U ratios ranging from 0.15 to 0.35. Twenty-two analyses performed in zircon outer parts (S3 Fig. 2) yield a concordia date of 58.9 ± 0.5/1.0 Ma (n = 22, MSWD = 1.4; Fig. 6C). The remaining data are slightly discordant because of the presence of a slight amount of common Pb (f206c > 0.1 %, Supplementary Table S4).

Zircon grains from the 755 Porphyry (sample BD5749-606 m) show variable U (250–1434 ppm) and Pb (16–125 ppm) contents, and Th/U ratios ranging from 0.18 to 0.36. Twenty-two analyses performed in zircon outer parts (S3 Fig. 2) yield a concordia date of 57.5 ± 0.2/0.9 Ma (n = 22, MSWD = 1.7; Fig. 6D). Two concordant analyses yield dates of around ~ 170 Ma (Fig. 6D) while two others yield dates around ~ 65 Ma (Fig. 6D). The remaining analyses are slightly discordant due to the presence of a slight amount of common Pb in the crystal lattice (f206c > 0.4 %, Supplementary Table S4).

Zircon crystals from the 8–110 Porphyry (sample BD5721-574 m) show high U (138–3593 ppm) and Pb (22–520 ppm) contents with Th/U ratios ranging from 0.11 to 0.49. Seventeen zircon U-Pb analyses performed in the inner and outer parts of the crystals (S3 Fig. 2) yield a concordia date of 56.5 ± 0.3/0.9 Ma (n = 17, MSWD = 1.3; Fig. 6E). One older ~ 63 Myr old zircon was analyzed (Fig. 6E). The remaining analyses are discordant because of the presence of common Pb in these grains (f206c up to 22.6 %, Supplementary Table S4).

Zircon grains from the newly discovered El Galo Porphyry (sample BD5764-826 m) show variable U (93–1340 ppm) and Pb (23–114 ppm) contents with Th/U ratios ranging from 0.16 to 0.42. Fifteen analyses were performed either in the inner or outer parts of the grains (S3 Fig. 2) and yield a concordia date of 56.1 ± 0.2/0.9 Ma (n = 15, MSWD = 1.2; Fig. 6F). Four concordant zircons yield dates of ~ 175 Ma, ~156 Ma, ~73 Ma and ~ 61 Ma, respectively (Fig. 6F). The remaining analyses have f206c > 0.3 % and are therefore discordant (Supplementary Table S4). We also sampled the Coarse-grained Porphyry which crosscuts the 8–110 Porphyry in the western part of the present-day pit (sample BC-22–13, Fig. 2 and 4D). However, we did not find any apatite or zircon, probably because it displays strong acidic hydrothermal alteration that could be responsible for the dissolution of the apatite and zircon grains. Probably for the same reason, we did not find apatite crystals in the Feldspar Porphyry.

4.3. Apatite U-Pb dating

Two new apatite U-Pb dates (Table 1) are reported for intrusive host rocks of the Buenavista del Cobre deposit (Tera-Wasserburg plots with apatite U-Pb lower intercept dates are reported in Figure 7 and data in Supplementary Table S5). Apatite grains from sample BD5753-627 m (Fig. 3C) are subhedral to anhedral with tabular and prismatic shapes (284–721 μm in size). For this sample, 37 apatite grains were analyzed.

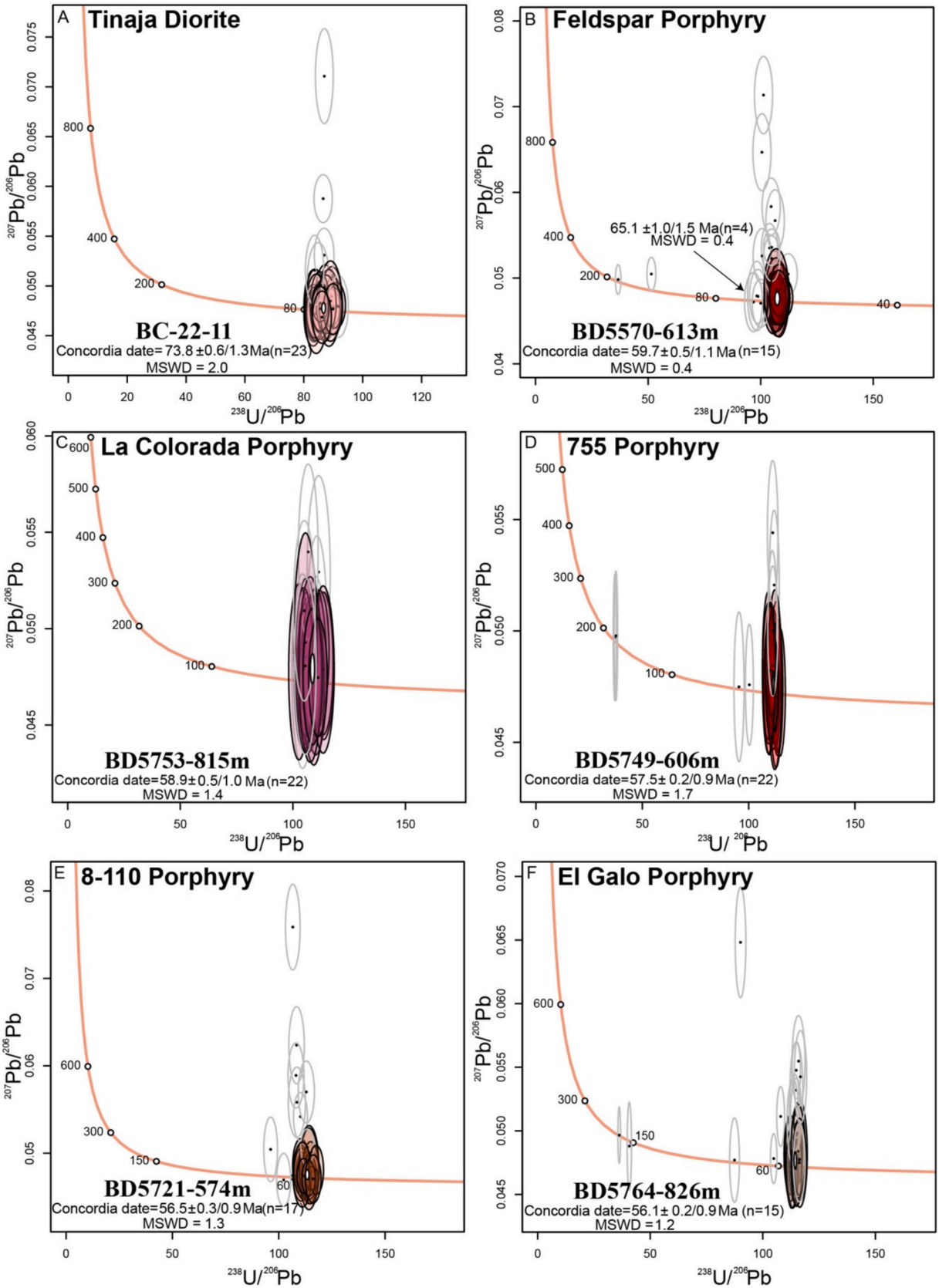

Fig. 6. Tera-Wasserburg concordia plots of zircon U-Pb analysis of the precursor batholith and main porphyries of the Buenavista del Cobre deposit. Colorless grains in the plot represent discordant ages and zircon inherited ages that were not considered in the calculation of the concordia date.

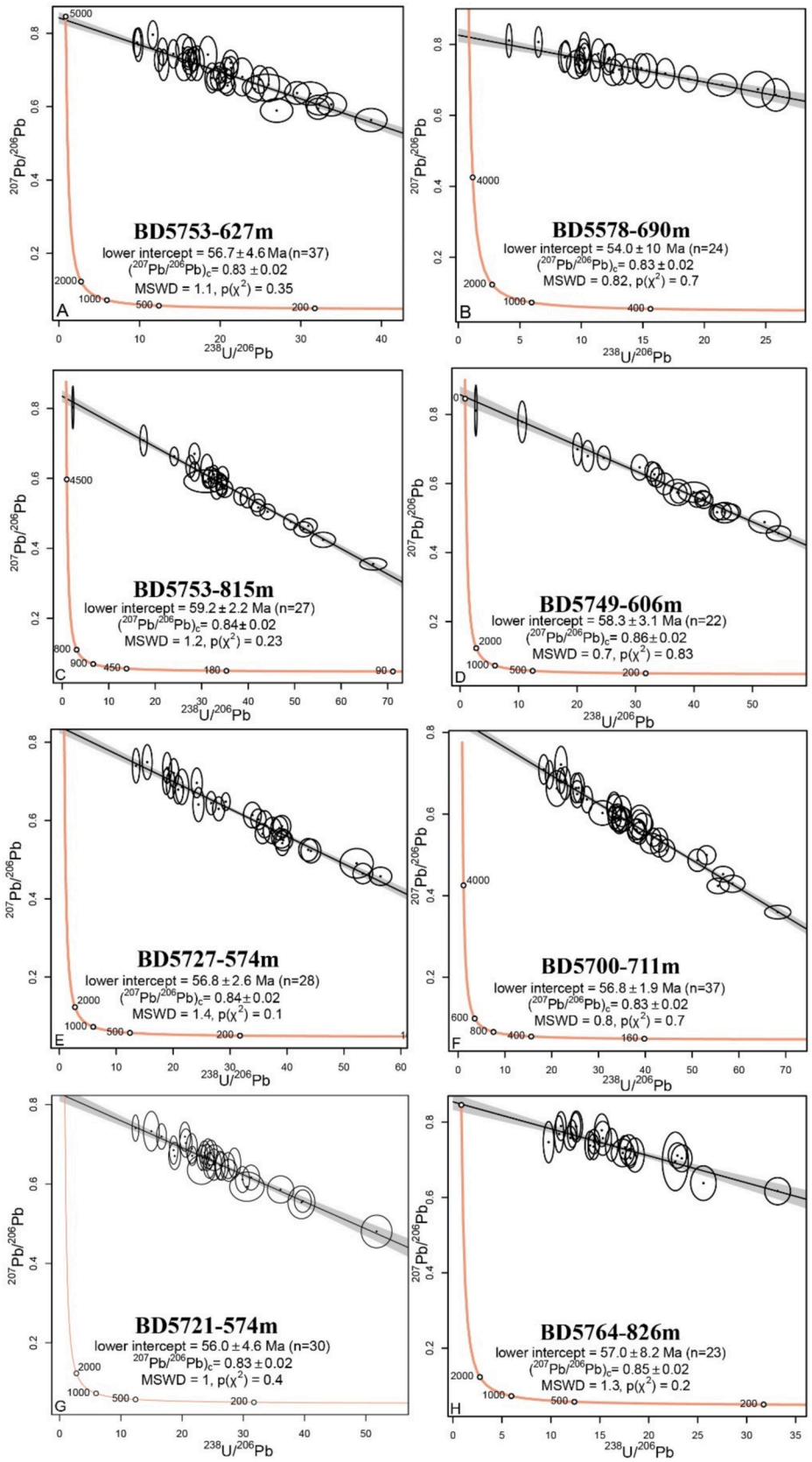

Fig. 7. Tera-Wasserburg discordia plots of apatite U-Pb data results of host rocks and ore-related porphyries.

They are characterized by high U (9 to 43 ppm) and homogeneous Pb (3 to 8 ppm) contents. In a Tera-Wasserburg diagram, they plot in a discordant position and yield a lower intercept U-Pb date of 56.7 ± 4.6 Ma (n = 37, MSWD = 1.1; Fig. 7A) with an initial common Pb value of $(^{207}Pb/^{206}Pb)_c = 0.83 \pm 0.02$. For sample BD5578-690 m, 24 analyses were performed. Apatite grains are mostly subhedral to anhedral with stubby, tabular and prismatic shapes (291–642 μm in size). They are characterized by fairly homogeneous U (3 to 34 ppm) and Pb (4 to 9 ppm) contents with variable Th/U ratios ranging from 0.05 to 1.93. Plotted in a Tera-Wasserburg diagram (Fig. 7B), they are all discordant and yield a lower intercept U-Pb date of 54.0 ± 10 Ma (n = 24, MSWD = 0.8; Fig. 7B) with a $(^{207}Pb/^{206}Pb)_c = 0.83 \pm 0.02$.

Apatite analyses from six samples from the ore-related porphyries yielded lower intercept apatite U-Pb dates ranging from 59.2 ± 2.2 to 56.0 ± 4.6 Ma (Table 1 and Fig. 7; apatite U-Pb data are available in Supplementary Table S5). In general, apatite grains from porphyry rocks are commonly subhedral to anhedral (225–927 μm in size) with broken-off tips and less commonly stubby and prismatic in shape. In the La Colorada Porphyry (sample BD5753-815 m) 27 apatites were analyzed. They have variable U (1–123 ppm) and more consistent Pb (4–9 ppm) contents with Th/U ratios ranging from 0.17 to 1.35. All the apatite U-Pb analyses plot in a discordant position and yield a lower intercept date of 59.2 ± 2.2 Ma (n = 27, MSWD = 1.2; Fig. 7C) with an initial common lead composition value of $(^{207}Pb/^{206}Pb)_c = 0.84 \pm 0.02$.

Apatite grains of the 755 Porphyry (sample BD5749-606 m) yield variable U (1–85 ppm) and more consistent Pb (2–9 ppm) contents with Th/U ratios ranging from 0.16 to 0.96. Twenty-two analyses define a discordia line with a lower intercept U-Pb date of 58.3 ± 3.1 Ma (n = 22, MSWD = 0.7; Fig. 7D) with $(^{207}Pb/^{206}Pb)_c = 0.86 \pm 0.02$.

The apatite grains from three samples from the 8–110 Porphyry yielded similar lower intercept apatite U-Pb dates (Fig. 7). Twenty-eight apatite grains were analyzed from sample BD5727-547 m. They have variable U (13–90 ppm) and Pb (6–17 ppm) contents with Th/U ratios ranging from 0.08 to 0.95. In the Tera-Wasserburg diagram, all the analyses plot in a discordant position and yield a lower intercept date of 56.8 ± 2.6 Ma (n = 28, MSWD = 1.4; Fig. 7E) with $(^{207}Pb/^{206}Pb)_c = 0.84 \pm 0.02$. Sample BD5700-711 m have apatite grains with variable U (14–118 ppm) and Pb (4–7 ppm) contents with Th/U ratios ranging from 0.08 to 2.61. Thirty-seven analyses define a discordia line with a lower intercept date of 56.8 ± 1.9 Ma (n = 37, MSWD = 0.8; Fig. 7F) with $(^{207}Pb/^{206}Pb)_c = 0.83 \pm 0.02$. Apatite crystals from sample BD5721-574 m have variable U (12–77 ppm) and Pb (3–9 ppm) contents with Th/U ratios ranging from 0.36 to 1.27. Thirty analyses yielded a lower intercept date of and 56.0 ± 4.6 Ma (n = 30, MSWD = 1.0; Fig. 7G) with $(^{207}Pb/^{206}Pb)_c = 0.83 \pm 0.02$.

Finally, the apatite grains from El Galo Porphyry (sample BD5764-826 m) have variable U (8–41 ppm) and consistent Pb (4–11 ppm) contents with Th/U ratios ranging from 0.15 to 4.44. A total of 23 analyses yielded a lower intercept U-Pb date of 57.0 ± 8.2 Ma (MSWD = 1.3; Fig. 7H) with $(^{207}Pb/^{206}Pb)_c = 0.85 \pm 0.02$.

4.4. Apatite trace element composition

Apatite trace element composition data are available in Supplementary Table S6. Concerning the intrusive host rocks, the REE distribution of apatite from sample BD5753-627 m shows a classical right-sloping REE pattern with an enrichment in LREE and a depletion in HREE (Fig. 8A) with $(La/Lu)_N$ ratios ranging from 1.2 to 15.3 (median of 2.1). Eu and Ce anomalies range from 0.3 to 0.8 (median 0.6) and from 1.1 to 1.3 (median 1.2), respectively. Apatite Cl concentrations are lower than 1.0 wt% (median 0.5 wt%), and Sr concentrations range from 198 to 372 ppm (median 256 ppm). Apatite of sample BD5578-690 m, another intrusive host rock, shows a relatively flat REE pattern (Fig. 8B) with $(La/Lu)_N$ ratios ranging from 0.4 to 4.5 (median 1.7). Eu anomalies and Ce anomalies range from 0.6 to 1.5 (median 0.9) and from 1.0 to 1.2 (median 1.1), respectively. Apatite Cl concentrations are below 0.7 wt% (median 0.4 wt%), and Sr concentrations range from 150 to 499 ppm (median 199 ppm).

In the ore-rich group, apatite from La Colorada Porphyry (BD5753-815 m) display a slightly enriched LREE pattern compared to HREE (Fig. 8C) with $(La/Lu)_N$ ratios ranging from 1.2 to 5.9 (median 1.6) and $(Ce/Yb)_N$ ratios ranging from 1.6 to 7.4 (median 2.1). This sample shows $(La/Sm)_N$ ratios ranging from 0.2 to 2.0 (median 0.8) and $(Dy/Yb)_N$ ratios ranging from 0.9 to 2.5 (median 1.2). Eu and Ce anomalies range from 0.3 to 1.4 (median 0.4) and from 1.0 to 1.3 (median 1.2), respectively. Apatite Cl concentrations are less than 0.6 wt% (median 0.4 wt%; Fig. 9) and the Sr concentrations range from 273 to 531 ppm (median 352 ppm). The 755 Porphyry apatite grains (BD5749-606 m) show a slightly enriched LREE pattern compared to HREE (Fig. 8D) with $(La/Lu)_N$ ratios ranging from 0.8 to 2.5 (median 1.5) and $(Ce/Yb)_N$ ratios ranging from 1.2 to 2.9 (median 1.9). The $(La/Sm)_N$ ratios are ranging from 0.3 to 2.0 (median 0.8) and $(Dy/Yb)_N$ ratios are ranging from 0.7 to 1.6 (median 1.2). Eu and Ce anomalies range from 0.3 to 1.0 (median 0.4) and from 1.1 to 1.2 (median 1.2), respectively. Apatite Cl concentrations are less than 0.6 wt% (median 0.4 wt%; Fig. 9) and Sr concentrations range from 183 to 489 ppm (median 332 ppm). Apatites from El Galo Porphyry (BD5764-826 m) display a convex REE pattern with a slightly enrichment in LREE compared to HREE (Fig. 8E) with $(La/Lu)_N$ ratios ranging from 1.9 to 3.3 (median 1.5) and $(Ce/Yb)_N$ ratios ranging from 1.4 to 4.4 (median 2.0). This sample shows $(La/Sm)_N$ ratios ranging from 0.4 to 1.2 (median 0.6) and $(Dy/Yb)_N$ ratios ranging from 1.3 to 1.8 (median 1.5). Eu and Ce anomalies range from 0.3 to 0.7 (median 0.4) and from 1.1 to 1.3 (median 1.2), respectively. Apatite Cl concentrations range from 0.1 to 0.6 wt% (median 0.4 wt%; Fig. 9) and the Sr concentrations range from 195 to 263 ppm (median 218 ppm).

In the ore-poor group, represented by the 8–110 Porphyry samples, apatite grains from sample BD5727-547 m display a right inclined REE pattern (Fig. 8F) with $(La/Lu)_N$ ratios ranging from 1.3 to 4.3 (median 2.3) and $(Ce/Yb)_N$ ratios ranging from 1.8 to 4.5 (median 2.7). This sample shows $(La/Sm)_N$ ratios ranging from 0.7 to 1.9 (median 1.0) and $(Dy/Yb)_N$ ratios ranging from 1.2 to 1.4 (median 1.3). Eu and Ce anomalies range from 0.3 to 0.4 (median 0.4) and from 1.0 to 1.3 (median 1.2), respectively. Apatite Cl concentrations are less than 0.5 wt % (median 0.3 wt%; Fig. 9), and Sr concentrations range from 310 to 356 ppm (median 332 ppm). In the case of sample BD5700-711 m, apatite grains show a right inclined REE pattern slightly enriched in LREE compared to HREE (Fig. 8G) with $(La/Lu)_N$ ratios ranging from 1.2 to 11.4 (median 2.6) and $(Ce/Yb)_N$ ratios ranging from 1.7 to 10.7 (median 3.2). The $(La/Sm)_N$ ratios are ranging from 0.5 to 2.9 (median 1.2) and $(Dy/Yb)_N$ ratios are ranging from 1.0 to 1.7 (median 1.2). Eu and Ce anomalies range from 0.4 to 0.9 (median 0.4) and from 1.1 to 1.3 (median 1.2), respectively. The apatite Cl concentrations are less than 0.4 wt% (median 0.2 wt%; Fig. 9), and the Sr concentrations range from 297 to 396 ppm (median 327 ppm). Apatite grains from sample BD5721-574 m display a right inclined apatite REE pattern (Fig. 8H) with $(La/Lu)_N$ ratios ranging from 1.3 to 6.1 (median 3.1) and $(Ce/Yb)_N$ ratios ranging from 1.2 to 5.8 (median 3.7). The $(La/Sm)_N$ ratios are ranging from 0.5 to 2.4 (median 1.1) and $(Dy/Yb)_N$ ratios are ranging from 1.1 to 1.5 (median 1.3). Eu and Ce anomalies range from 0.3 to 0.6 (median 0.3) and from 0.8 to 1.3 (median 1.2), respectively. The apatite Cl concentrations are less than 0.4 wt% (median 0.2 wt%; Fig. 9) and the Sr concentrations range from 303 to 361 ppm (median 328 ppm).

5. Discussion

5.1. Host rocks geochronology

New zircon U-Pb dates obtained from the intrusive host rock of the mineralization help to support and discuss the geological observations made by several authors over the years. Sample BD5753-468 m was collected from a deep exploration drill hole (Fig. 2) in the present mine operation and corresponds to a coarse-grained granitic rock that is

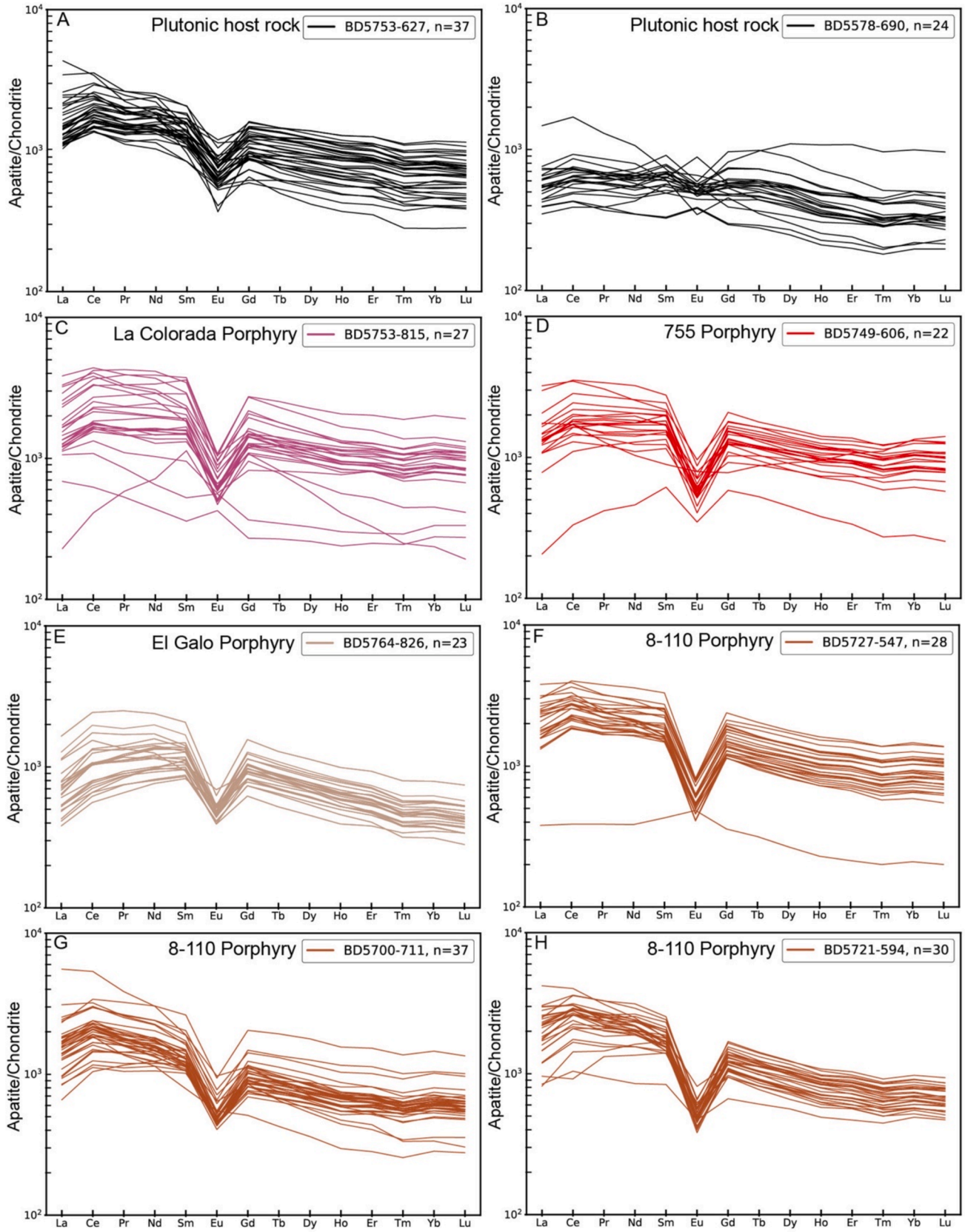

Fig. 8. Chondrite-normalized apatite REE patterns of the intrusive host rocks and main porphyries of Buenavista del Cobre deposit. A) Sample BD5753-627 m displays a classical right-sloping REE pattern. B) Sample BD5578-690 m from a Jurassic pluton has a flat apatite REE pattern. Diagrams C, D, and E represent the apatite REE distributions from the ore-rich group (La Colorada, 755 and El Galo porphyries, respectively), displaying relatively flat to upward convex apatite LREE distributions. Diagrams F, G, and H are apatite REE patterns from the ore-poor group (8–110 Porphyry) and show right-sloping REE patterns with an enrichment in LREE compared to HREE. Chondrite values are from Barrat et al. (2012).

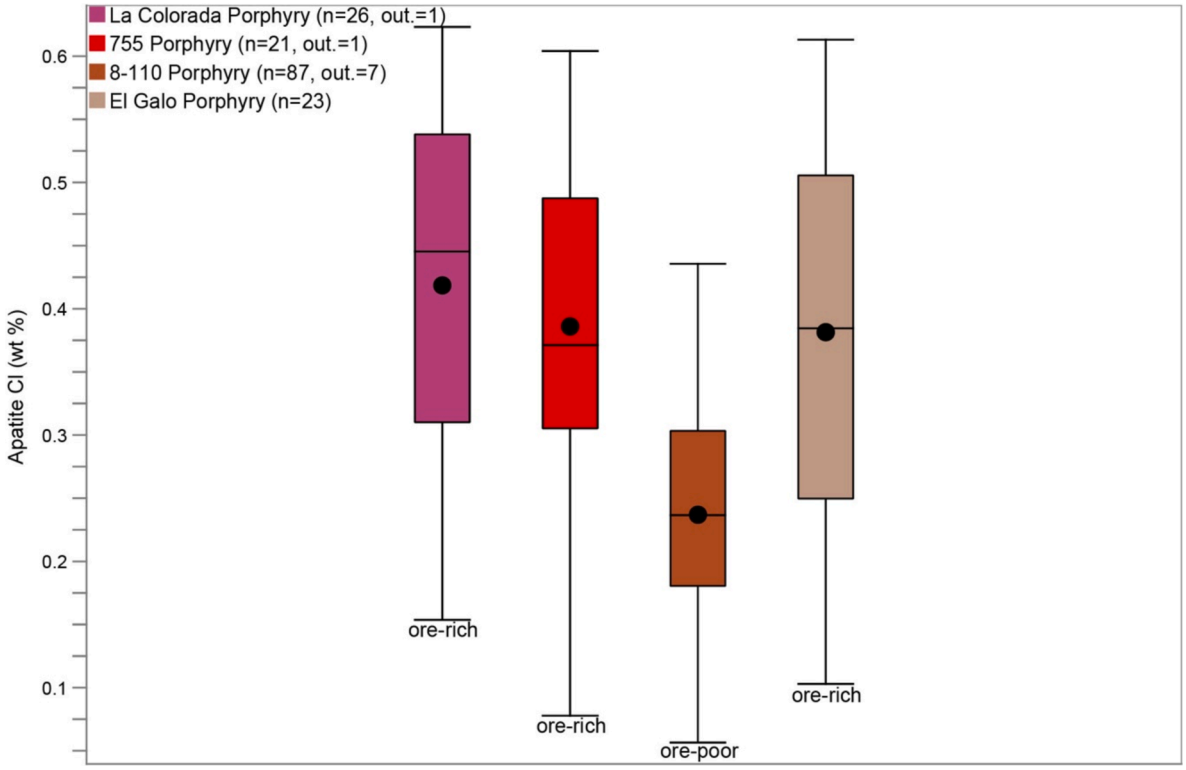

Fig. 9. Box plots showing the apatite chlorine composition for ore-rich and ore-poor porphyry intrusions. The central box is the middle 50% of data from the first (bottom of the box) and third (top of the box) quartiles. The black circle and line are the mean and median of the data, respectively. The whiskers are the extreme values that are not outliers. Outliers values (out.) were discarded for this comparison. Porphyries are organized from older (left) to younger (right).

unconformably overlain by the Henrietta Formation. This sample yielded an upper intercept age of 1422 ± 14/18 Ma (Fig. 5A). The upper intercept date is equivalent to the upper intercept age of 1440 ± 15 Ma reported by Anderson and Silver (1977) for the Cananea Granite in the Capote Basin. We therefore interpret it as the emplacement age of the Cananea Granite, confirming the Precambrian age of this intrusive. In the case of the lower intercept age (111 ± 9/9 Ma; Fig. 5A), no tectonomagmatic event that could explain lead loss has been recognized yet in the Cananea Mining District at the end of the Lower Cretaceous. For this reason, we believe that the lower intercept age recorded by the Cananea Granite possibly has no geological meaning.

To date, the only known outcrop of the Cananea Granite in the Cananea Mining District occurs in the Capote Basin (Valentine, 1936), where it is unconformably overlain by the Paleozoic strata and bordered by the NW-SE oriented Elisa and Capote Pass faults. In the Capote Basin, Zn-Cu skarns mineralization developed in the Paleozoic rocks associated with the emplacement of the Late Cretaceous-Paleogene magmatic-hydrothermal systems (Meinert, 1980, Farfán-Panamá, 2002; Ortiz-Olvera, 2022). Recently, the Capote Pass fault has been interpreted as an Oligo-Miocene south-dipping normal fault (Ortiz-Olvera, 2022). If this fault displaced the Cananea Granite to the south, as suggested by its recognition in drill hole exploration, then the Paleozoic sequence and its associated skarn mineralization might be present below the Mesa and Henrietta Formations, east of the current open pit operation (Fig. 2). This new finding highlights the importance of dating newly discovered intrusive bodies as it could have important consequences, in this case increasing the possibility of finding previously undiscovered Zn-Cu skarns deposits.

The presence of Triassic-Jurassic igneous rocks in the region of Cananea Mining District has been proposed by several authors (e.g., Valentine, 1936; Meinert, 1980; Wodzicki, 1995). These rocks include the volcanic rocks of the Elenita and Henrietta Formations and the El Torre Syenite pluton. This assumption was made on the basis of cross-cutting relationships between different rock units and their lithological similarities to rocks of Triassic-Jurassic age in southern Arizona. For example, the Elenita Formation was correlated with the Late-Triassic to Mid-Jurassic Mt. Wrightson Formation, which crops out in Santa Rita Mountains, Arizona (Drewes, 1971). Despite the contact between Elenita Formation and Henrietta formation being a fault, clasts of the Elenita Formation were reported by Valentine (1936) in the lowermost Henrietta Formation, which was therefore considered to be younger. Previous attempts of $^{40}Ar/^{39}Ar$ hornblende dating of the Henrietta Formation yielded ages of 57.9 ± 0.2 Ma and ~ 94 Ma, which were interpreted as a thermally reset age and a minimum formation age for this unit (Wodzicki, 1995). In this study, we report for the first time a zircon U-Pb age of 186.8 ± 1.1/3.0 Ma (Fig. 5C) that was obtained for a volcanic flow from the Henrietta Formation (Fig. 2), confirming an Early Jurassic age for these rocks.

In addition, a Jurassic age has been proposed for the El Torre Syenite pluton based on its lithologic and geochemical similarities to the granitic to syenitic plutons emplaced from 170 to 150 Ma in Sonora (Gastil et al., 1978; Anderson and Silver, 1978; Meinert, 1980; Wodzicki, 1995). An $^{40}Ar/^{39}Ar$ hornblende age of 58.4 ± 0.5 Ma for this rock was interpreted as reset age due to its similarity with the age of porphyry copper mineralization of the district, whereas a ~ 70 Ma date was interpreted as a minimum formation age with a poorly defined plateau (Wodzicki, 1995). In this study, samples BD5752-669 m and BD5578-690 m from two plutonic rocks intersected at depth by two exploration drill holes (Fig. 2), yielded zircon U-Pb ages of 186.9 ± 1.3/3.1 Ma (Fig. 5B, Table 1) and 176.3 ± 1.1/2.9 Ma (Fig. 5D, Table 1), respectively. Specifically, sample BD5578-690 m corresponds to a medium to fine-grained plutonic rock and is composed dominantly by K-feldspar + plagioclase + hornblende ± quartz ± biotite and accessory zircon and apatite (Fig. 3E). This composition is similar to the mineralogical composition described for the El Torre Syenite (Valentine, 1936; Meinert, 1982) and we thus argue for an Early Jurassic age for this intrusion.

In addition, the new apatite U-Pb ages obtained in this study from intrusive host rocks are 56.7 ± 4.6 Ma (sample BD5753-627 m, Fig. 7A, Table 1) and 54.0 ± 10.0 Ma (sample BD5578-690 m, Fig. 7B, Table 1), and are in accordance with the previously published $^{40}Ar/^{39}Ar$ age. We therefore interpret these ages as thermally reset ages due the effects of the porphyry emplacement. For this reason, we prefer not to discuss apatite geochemistry of host rocks in this study because of the possible compositional re-equilibration of apatites during high-temperature hydrothermal alteration.

The Jurassic zircon U-Pb ages we obtained for both volcanic and plutonic rocks in the Buenavista del Cobre deposit evidence the presence of an Early Jurassic magmatic arc at Cananea latitude (Anderson and Silver, 1978; Tosdal et al., 1989; Valencia-Moreno et al., 2024). It has to be noted that Jurassic porphyry copper mineralization associated with a Jurassic arc magmatism has been reported ~ 65 km northeast of the Buenavista del Cobre deposit in Bisbee, Arizona, and throughout southwestern North America (Barton et al., 2011). The recognition of an Early Jurassic volcano-plutonic system in the Buenavista del Cobre deposit opens the possibility of the development of a contemporaneous magmatic-hydrothermal system. However, further evidence is needed to confirm the existence of such an event.

Several authors have suggested that the Tinaja Diorite and the Cuitaca Granodiorite are part of the same batholitic body and that they are the precursor magmas of the porphyry copper mineralization at Cananea Mining District (Valentine, 1936; Meinert, 1982; Bushnell, 1988; Wodzicki, 1995; Santillana-Villa et al., 2021). Limited geochronological data preclude establishing a temporal relationship between these intrusions. The Cuitaca Granodiorite has a zircon U-Pb age of ~ 64 Ma (Anderson and Silver, 1977; Del Rio-Salas et al., 2017). Our new zircon U-Pb age of 73.8 ± 0.6/1.3 Ma (sample BC-22–11, Fig. 6A, Table 1) for the Tinaja Diorite reveals that this intrusion was emplaced ~ 10 Ma earlier than the Cuitaca Granodiorite. Thus, we interpret the previously reported $^{40}Ar/^{39}Ar$ hornblende age of 63.0 ± 0.4 Ma for the Tinaja Diorite (Wodzicki, 1995) as a thermally reset age due to the intrusion of the Cuitaca Granodiorite at ~ 64 Ma. In addition, a similar age of ~ 74 Ma (Del Río-Salas et al., 2017) was obtained for the precursor pluton at the El Pilar deposit, ~40 km northwest of the Buenavista del Cobre deposit (Fig. 1). Together, these data suggest that the Tinaja Diorite and El Pilar intrusive rocks probably represent the onset of the magmatism related to the precursor magmas of the main porphyry systems at the Cananea Mining District at ~ 74 Ma.

5.2. *Multiple magmatic events*

Giant porphyry copper deposits around the world, such as Chuquicamata (Reynolds et al., 1998; Ballard et al., 2001), El Salvador (Gustafson and Hunt, 1975; Lee et al., 2017), El Teniente (Maksaev et al., 2004), and Bajo de la Alumbrera (Harris et al., 2004 and 2008) are the product of multiple superimposed magmatic events as indicated by zircon U-Pb dating of ore-related porphyry intrusions. However, it is known that differences in emplacement ages between the different porphyries that make up a porphyry copper deposit can be difficult to determine, even with high-resolution methods such as zircon U-Pb SHRIMP analyses (e.g., Lee et al., 2017). Therefore, further geological evidences such as cross-cutting relationships between porphyry intrusions with different mineralogy, texture and/or geochemistry, as well as dating of minerals associated with alteration and mineralization are needed to reconstruct the emplacement timing of the different intrusions.

Zircon grains from the Buenavista del Cobre porphyry rocks exhibit needle-like shapes with a concentric oscillatory growth zoning (S3 Fig. 2), typical of magmatic zircon that crystallized in rapidly cooling intrusions (Corfu et al., 2003; Nathwani et al., 2023). In addition, most zircons have similar ages in the inner and outer parts of the grains, suggesting no effects of zircon recrystallization on inherited grains. For these reasons, we interpret the zircon U-Pb dates of the main cluster of concordant analyses as the emplacement ages of the different porphyry intrusions. These new zircon U-Pb ages of porphyry rocks obtained in this study do not allow us to clearly differentiate in time discrete magmatic pulses for the Buenavista del Cobre deposit, as all ages overlap within the analytical error at 2σ level (Fig. 10). However, as mentioned before, several porphyry phases have been recognized in the Buenavista del Cobre deposit, which are distinguished by their cross-cutting relationships, mineralogical compositions, textures, and their ore-poor/ore-rich natures (Valentine, 1936; Ochoa-Landín and Echávarri-Pérez, 1978; Ochoa-Landín and Navarro-Mayer, 1979). Considering all the disponible data, the proposed sequence of porphyry intrusions is as follows: Feldspar Porphyry, La Colorada, 755, 8–110, and El Galo porphyries, and finally the Coarse-grained Porphyry phase. Hereunder, we review the different arguments used to establish this chronology.

The Feldspar Porphyry yields a zircon U-Pb age of 59.7 ± 0.5/1.1 Ma, which is indistinguishable from the La Colorada Porphyry that yields a zircon U-Pb age of 58.9 ± 0.5/1.0 Ma (Fig. 10). A second group of dates from the Feldspar Porphyry, corresponding to four concordant analyses, yield a concordia date of 65.1 ± 1.0/1.5 Ma (n = 4, MSWD = 0.4; Fig. 6B). This date is fairly similar to the emplacement age of ~ 64 Ma of the Cuitaca Granodiorite (a precursor magma of the porphyry magmas) elsewhere in the Cananea Mining District (Anderson and Silver, 1977; Del Rio Salas et al., 2013). We thus suggest that this older group corresponds to zircon grains that formed at depth in the Cuitaca magmatic chamber and were dragged-up to shallower crustal levels during the emplacement of the Feldspar Porphyry. Moreover, both zircon U-Pb ages of the Feldspar and La Colorada porphyries correlate with the molybdenite Re-Os ages of 59.2 ± 0.3 Ma for a chalcopyrite + pyrite + molybdenite (massive) mineral association at the top of the La Colorada breccia pipe, and of 59.3 ± 0.3 Ma for a disseminated style mineralization (Barra et al., 2005; Fig. 10). In the case of the disseminated style Re-Os mineralization age, it is possible that the emplacement of the Feldspar Porphyry marks the onset of mineralization at the Buenavista del Cobre deposit at 59.3 ± 0.3 Ma. Yet, further work on the mineralization associated with the Feldspar Porphyry emplacement is required to confirm or infer this possibility. Indeed, since the Feldspar Porphyry is considered an ore-poor porphyry and is not spatially related to the La Colorada breccia pipe, it cannot be associated with the main Cu-Mo mineralization event associated with the formation of this breccia (Ochoa-Landín and Navarro-Mayer, 1979; Fig. 10). In contrast, the La Colorada Porphyry is classified as an ore-rich intrusion (Fig. 10), which occurs in a close spatial relationship to the La Colorada breccia pipe (Perry, 1935). Additionally, the early potassic alteration in the La Colorada breccia pipe (Bushnell, 1988) was dated by K/Ar on phlogopite at 59.9 ± 2.1 Ma and 58.5 ± 2.1 Ma (Damon and Mauger, 1966; Varela, 1972). These ages correlate well with the lower intercept apatite U-Pb

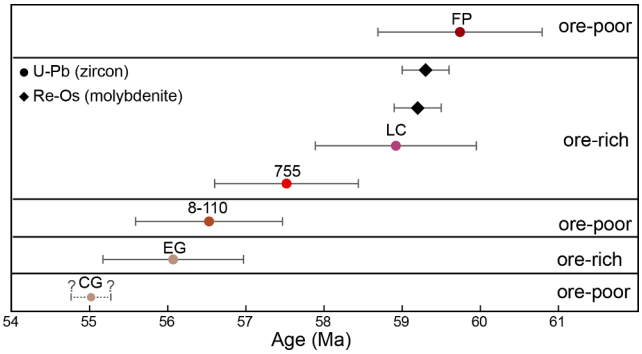

Fig. 10. Emplacement (zircon U-Pb ages) and Cu-Mo mineralization timing (Re-Os ages by Barra et al., 2005) of the six known porphyry intrusions in the Buenavista del Cobre deposit. Error bars on zircon U-Pb data correspond to propagated systematics uncertainties. Abbreviations: FP (Feldspar Porphyry), LC (La Colorada Porphyry), 755 (755 Porphyry), 8–110 (8–110 Porphyry), EG (El Galo Porphyry), CG (Coarse-grained Porphyry).

age of 59.2 ± 2.2 Ma (sample BD5753-815 m, Fig. 7C, Table 1) obtained for the La Colorada Porphyry and suggest that the main Cu-Mo mineralization event at Buenavista del Cobre began with the emplacement of the La Colorada Porphyry at 58.9 ± 0.5/1.0 Ma (zircon U-Pb emplacement age of sample BD5753-815 m, Fig. 6C and 10, Table 1), after the emplacement of the ore-poor Feldspar Porphyry at 59.7 ± 0.5/1.1 Ma (zircon U-Pb emplacement age for sample BD5570-613 m, Fig. 6B and 10, Table 1).

In the case of the 755 Porphyry, we obtained a zircon U-Pb age of 57.5 ± 0.2/0.9 Ma (Fig. 6D) and an apatite U-Pb age of 58.3 ± 3.1 Ma (Fig. 7D). The zircon U-Pb age overlaps with the La Colorada Porphyry emplacement age but postdates the Feldspar Porphyry emplacement age (Fig. 10). This observation is in good agreement with the fact that the 755 Porphyry crosscuts the Feldspar Porphyry and that it shares apatite geochemical characteristics with the ore-rich La Colorada Porphyry (cf. next section). One possible interpretation is that the La Colorada and the 755 porphyries belong to a single porphyry complex originating the main Cu mineralization event. Alternatively, these porphyries could correspond to two different intrusions that were emplaced in a relatively short period of time (as described for the L and K porphyries in the El Salvador deposit; Gustafson and Hunt, 1975; Lee et al., 2017), making it impossible to differentiate their emplacement ages by our dating methods. Interestingly, it has to be noted that the 755 Porphyry zircon U-Pb emplacement age does not overlap with the molybdenite Re-Os ages of the main Cu mineralization event related to the La Colorada Porphyry emplacement (Fig. 10). We thus consider that the emplacement of the 755 Porphyry corresponds to a different magmatic pulse that might have developed a magmatic-hydrothermal system associated with a second Cu-Mo mineralization event. However, further works on Re-Os and $^{40}Ar/^{39}Ar$ geochronology on ore-related minerals are needed to confirm this interpretation.

The 8–110 Porphyry yields a zircon U-Pb age of 56.5 ± 0.3/0.9 Ma (sample BD5721-574 m, Fig. 6E, Table 1) and three apatite U-Pb ages of 56.8 ± 2.6 Ma (sample BD5727-547 m, Fig. 7E, Table 1), 56.8 ± 1.9 Ma (sample BD5700-711 m, Fig. 7F, Table 1), and 56.0 ± 4.6 Ma (sample BD5721-574 m, Fig. 7G, Table 1). Additionally, the El Galo Porphyry yields a zircon U-Pb age of 56.1 ± 0.2/0.9 Ma (sample BD5764-826 m, Fig. 6F, Table 1) and an apatite U-Pb age of 57.0 ± 8.2 Ma (Fig. 7H, Table 1). Considering the propagated error uncertainties, these intrusions (8–110 and El Galo porphyries) are thus temporally indistinguishable from the 755 Porphyry (Fig. 10), impeding defining different discrete igneous events of emplacement.

However, the 8–110 Porphyry has historically been classified as an ore-poor porphyry (Ochoa-Landín and Navarro-Mayer, 1979; Fig. 10) and exhibits apatite geochemistry differences from the 755 and El Galo ore-rich porphyries (cf. next section). We also show that the El Galo Porphyry emplacement is spatially associated with an ore-rich potassic alteration zone (Fig. 4F), and that it shares apatite geochemical characteristics with the ore-rich porphyries (La Colorada and 755 porphyries; cf. next section). Taken together, these observations suggests that the emplacement of the El Galo Porphyry is related to a different magmatic-hydrothermal system than the 8–110 Porphyry.

Moreover, the maximum age of the Cu-Mo mineralization event associated with the El Galo Porphyry potassic alteration is constrained to 56 Ma as Cu and Mo sulfides veinlets cross-cut the El Galo Porphyry (Fig. 4E), which has a 56.1 ± 0.2/0.9 Ma crystallization age (Fig. 6F, Table 1). This is younger than the available molybdenite Re-Os ages associated to the emplacement of the La Colorada Porphyry and breccia (see above, Fig. 10). Even if there is no molybdenite Re-Os date to further constrain this young mineralizing hydrothermal system, we consider that at least two discrete events of mineralization occurred at Buenavista del Cobre, associated with the emplacement of the La Colorada Porphyry for the first event and with the El Galo Porphyry for the younger event (note that it is possible that another mineralizing event occurred associated with the emplacement of the 755 Porphyry).

Finally, the Coarse-grained Porphyry is an ore-poor porphyry intrusion, which is likely younger than the 8–110 and El Galo porphyries as it crosscuts the 8–110 Porphyry (Ochoa-Landín and Navarro-Mayer, 1979; Fig. 10). Unfortunately, we did not find any apatite and zircon crystals in this porphyry and were unable to further characterize this intrusion.

5.3. Geochemistry of apatite as a fertility indicator

5.3.1. Magmatic oxidation state

Apatite prefers to incorporate Eu^{3+} and Ce^{3+} rather than Eu^{2+} and Ce^{4+} because the difference in ionic radius between them and Ca^{2+} is small and they can substitute for it (Sha and Chappell, 1999; Cao et al., 2012; Pan et al., 2016). Moreover, the redox ratios Eu^{2+}/Eu^{3+} and Ce^{3+}/Ce^{4+} of a melt is a function of oxygen fugacity, temperature, pressure and composition of the melt (Sha and Chappel, 1998). Oxidized melts with high oxygen fugacity and low Eu^{2+}/Eu^{3+} ratios have higher Eu^{3+} abundance than reduced melts. As apatite preferentially incorporate Eu^{3+}, apatites crystallizing from oxidized melts are expected to present higher Eu content and thus a lower Eu anomaly than apatites crystallizing from reduced melts. The same reasoning can be done for Ce in apatite: Ce^{3+}/Ce^{4+} of oxidized melts is low and their Ce^{3+} content (which preferentially partitions in apatite) is low, thus apatites crystallizing from an oxidized melt are expected to exhibit low Ce content and thus higher Ce anomalies than apatites from reduced melts. As a result, apatite chemistry has been used as a proxy for the oxidation state of magmas using Eu and Ce anomalies (e.g., Sha and Chappell, 1999; Cao et al., 2012; Pan et al., 2016).

In Buenavista del Cobre, the Eu and Ce anomalies (Eu/Eu* and Ce/Ce* values) of apatite from ore-rich and ore-poor intrusions overlap with no clear difference between the two groups (Fig. 11A). These results suggest that the magmatic oxidation states of the porphyritic magmas were similar and that Eu and Ce anomalies cannot be used in our case as good fertility indicators to distinguish ore-rich from ore-poor magmas. This also suggests that other factors such as the magma H_2O content are more important at the deposit scale than the magma oxidation state (e.g., Richards, 2011).

5.3.2. Apatite REE signature

In contrast to the relative oxidation state of the magmas, an evaluation of the general apatite REE composition of ore-rich and ore-poor porphyries allows us to distinguish two fields with specific $(La/Sm)_N$ and $(Ce/Yb)_N$ signatures (Fig. 11B). As REE are incompatible elements, and because LREE are more incompatible than HREE, these values allow to track the relative differentiation of melts. Apatites from the ore-poor group show a more fractionated REE distribution ($(Ce/Yb)_N = 1.2–10.7$; median 3.1) with a slight LREE enrichment compared to apatites from the ore-rich group ($(Ce/Yb)_N = 1.2$ to 7.4; median 2.0). In addition, the ore-poor apatite show a higher LREE concentrations and MREE depletion with higher $(La/Sm)_N$ ratios (0.5 to 2.9; median 1.1) than apatites from ore-rich porphyries ($(La/Sm)_N = 0.2$ to 2.0; median 0.8). These findings suggest that the ore-poor porphyries experienced a higher degree of LREE fractionation and therefore, a higher degree of magmatic differentiation compared to ore-rich porphyries. However, this interpretation is at odds with the fact that Cu is an incompatible element and should concentrate in the melts the more differentiated from the parental magma (e.g., Richards 2003). We instead propose that the apatite trace element composition difference between ore-rich and ore-poor magmas is controlled by petrogenetic processes such as crystal fractionation of specific REE-bearing and hydrous or anhydrous mineral phases in the parental melt (eg., Sha and Chappell, 1999; Sun et al., 2022; Quan et al., 2023). Indeed, mineral fractionation is known to influence the concentration of REE and volatiles such as the H_2O in residual magmas which affects the transport of metals and magma fertility. We explore this possible interpretation in the next section.

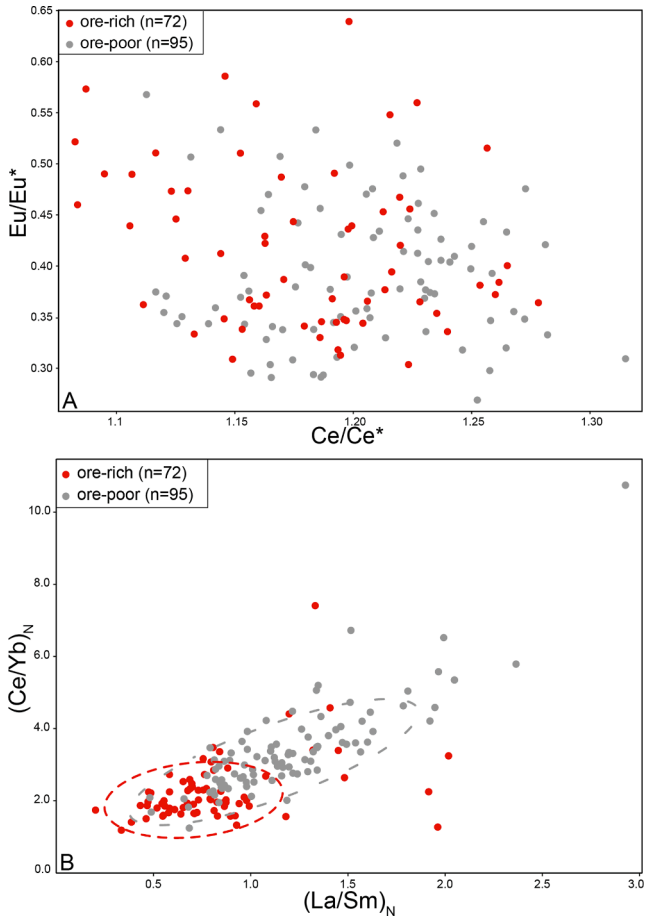

Fig. 11. Apatite Ce vs Eu anomalies and $(La/Sm)_N$ vs $(Ce/Yb)_N$ ratios plots. Red and gray dotted lines represent the Mahalanobis contour ellipses with a p-value = 0.95 showing the data outliers for the ore-rich and ore-poor groups, respectively.

5.3.3. *Fractional crystallization process of porphyry magmas sources*

Apatite trace element content (such as Sr, Th, U, and REE) can be used as a geochemical index to trace the mineral crystallization sequence involved in the petrogenesis of granitic rocks (Nathwani et al., 2020; Sun et al., 2022; Quan et al., 2023), which may control the fertility of porphyritic magmas. Indeed, trace elements composition of apatite depends on the mineral phases that crystallized before or at the same time as apatite (e.g., Pan et al., 2016; Nathwani et al., 2020; Zhang et al., 2020; Sun et al., 2022; Quan et al., 2023). In particular, accessory minerals such as monazite, allanite, titanite, and zircon can incorporate REE, U, and Th in their crystalline structure and compete with apatite during magma crystallization (Sha and Chappell, 1999; Sun et al., 2022 and references therein).

In Buenavista del Cobre, apatite grains from ore-rich and ore-poor groups, show positive correlation between REE and Th, and between REE and U (Fig. 12); suggesting the co-crystallization of accessory minerals that may compete with apatite incorporating these elements (Sha and Chappell, 1999; Sun et al., 2022 and references therein). The crystallization of monazite, which could play a role in Th incorporation, is unlikely because of the calc-alkaline nature of the porphyry magmas, an unusual environment for monazite crystallization (Sha and Chappell, 1998). Moreover, experimental studies suggest that zircon typically crystallizes later than apatite during the cooling of continental arc magmas (e.g., Lee and Bachmann, 2014), limiting the influence of zircon crystallization on the U and Th composition of apatite. Allanite may also crystallize at the same time or before apatite, incorporating REE as well as Th. Actually, the normalized apatite REE patterns of all samples show a depletion in La (Fig. 8C-H) and a positive correlation between Th and total REE composition (Fig. 12), which are consistent with allanite crystallization (e.g., Cao et al., 2012; Quan et al., 2023). Finally, if titanite crystallizes before or at the same time as apatite, the composition of the latter will show a positive correlation between U and total REE composition (Quan et al., 2023; Fig. 12). Titanite crystallization is typical of oxidized magmas (Wones, 1989). Our results are thus in agreement with the relatively high oxidation state expected for the source of porphyry magmas. However, if crystal fractionation of titanite and allanite in the parental magma promotes the formation of porphyritic melts (e.g., Cao et al., 2012), it does not have any effect on the porphyry magmas fertility (both ore-poor and ore-rich porphyries show titanite and allanite fractionation signature) because it only controls the REE budget of the magma, which does not affect metal solubility.

In porphyry copper deposits, metal solubility increases with the H_2O content of causative magmas. The initial H_2O content of a melt is related to its origin at deep crustal levels (in the MASH zone; Cloos, 2001; Richards, 2003 and 2011; Sillitoe, 2010). At shallower crustal levels, in the parental magma chamber, crystallization of anhydrous minerals such as plagioclase tends to increase the H_2O content of the residual magma, whereas crystallization of hydrous minerals such as hornblende removes H_2O from the melt (Cloos, 2001; Tosdal and Richards, 2001). On one hand, when apatite crystallizes from a melt dominated by plagioclase fractionation, Sr and to a lesser extent LREE tend to be retained in plagioclase, which induces a large spread in apatite Sr contents (Sha and Chappell, 1999; Belousova, 2001; Pan et al., 2016: Sun et al., 2022; Quan et al., 2023). On the other hand, hornblende tends to incorporate MREE, and when apatite crystallizes from a melt dominated by hornblende fractionation, apatite will exhibit a large spread in the $(La/Sm)_N$ ratios as consequence of MREE depletion (Sun et al., 2022).

In the Buenavista del Cobre porphyritic bodies, apatite commonly occurs as sub-rounded inclusions within major minerals (quartz, feldspars and hornblendes; S1 Fig. 3) suggesting that apatite crystallized at depth and were transported by the porphyritic melt. If this interpretation is correct, the apatite chemistry must reflect the petrogenetic processes that occurred at depth, and at the origin of the different metal budgets of the porphyritic magmas. The ore-poor 8–110 Porphyry yielded apatite showing a hornblende fractionation signature (Fig. 12), whereas all the apatites from ore-rich porphyry intrusions show Sr contents and REE patterns indicating plagioclase fractionation (Fig. 12). This can be explained by the fact that crystallization of hydrated mineral phases such as hornblendes at depth results in a low-fluid content residual melt, lowering the potential of magmatic-hydrothermal activity and inhibiting metal mobilization, fluid exsolution and mineralization at shallow crustal levels (Fig. 13). In contrast, crystallization at depth of anhydrous mineral phases such as plagioclase increases the fluid content of the residual melt, which in turn increases metal mobilization and promotes high-grade mineralization in hydrothermal systems at shallower crustal levels (Fig. 13). Thus, we interpret that in the Buenavista del Cobre deposit the ore-poor and ore-rich porphyry magmas are the product of parental magmas in which hornblende and plagioclase crystallized, respectively.

5.3.4. *Apatite Cl content*

The Cl content of the porphyry magmas is often used to assess their fertility because Cl forms complexes with metals such as Cu and determines the metal transport capacity of magmas and hydrothermal fluids (e.g., Shinohara, 1994; Williams et al., 1995; Chelle-Michou and Chiaradia, 2017). Apatite can record the volatile content of magmas due to its ability to incorporate elements such as Cl, S and F (e.g., Sha and Chappell, 1999). Figure 9 shows the variation in apatite chlorine content of the different porphyry intrusions at the Buenavista del Cobre deposit. During the first fertile stage of Cu-Mo mineralization, the La Colorada and the 755 ore-rich porphyries have slightly high apatite Cl (median = 0.4 wt%) concentrations (Fig. 9). Subsequently, the ore-poor 8–110 Porphyry emplacement is associated with a slightly lower apatite Cl

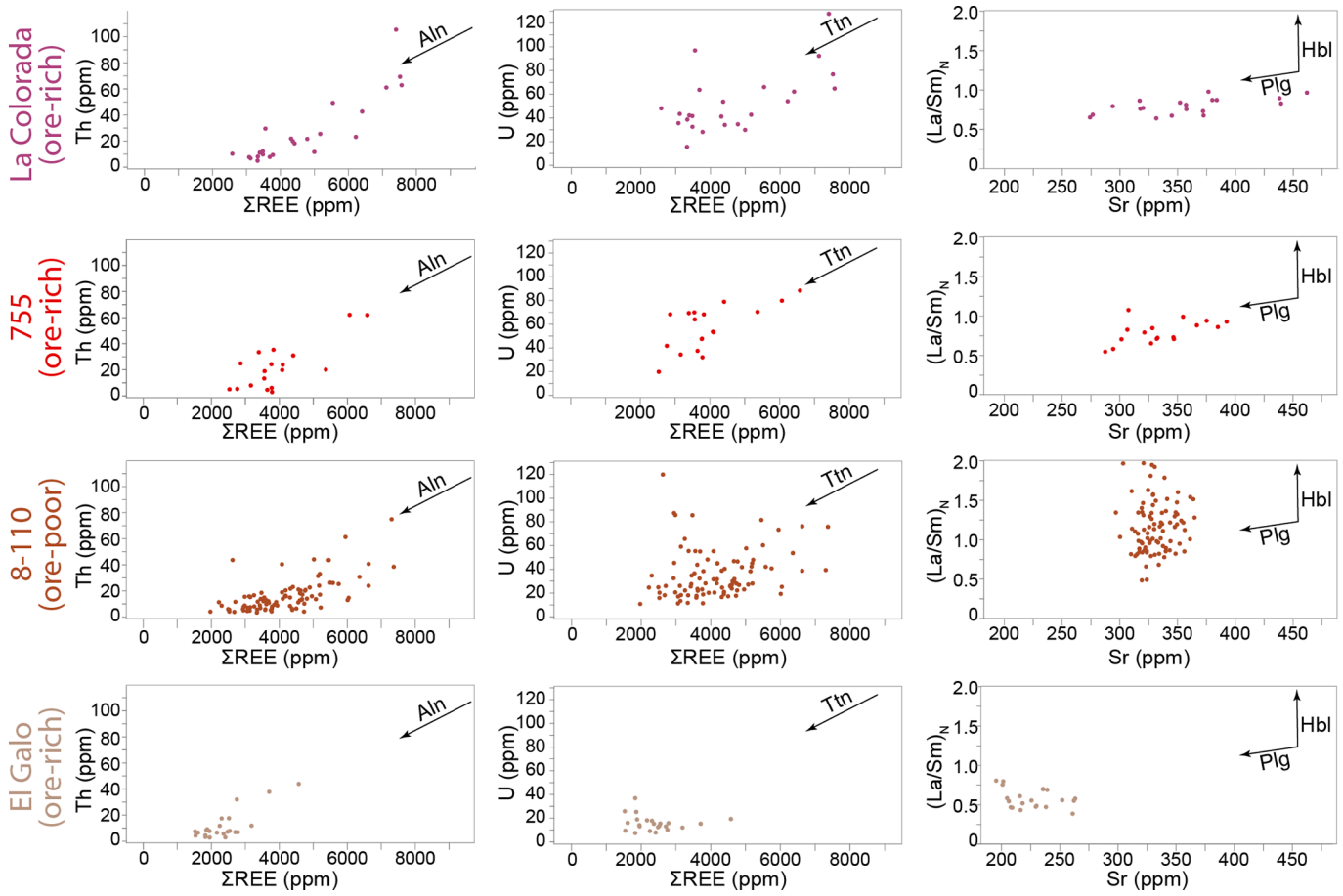

Fig. 12. Different plots used to track the fractionation of different mineral phases that compete with apatite for trace element incorporation (REE composition, $(La/Sm)_N$ ratios, Sr, U and Th concentrations). Abbreviations: Aln = alanite; Ttn = titanite.

concentrations (median = 0.2 wt%). The apatite Cl concentration increases again (median = 0.4 wt%) with the emplacement of the El Galo ore-rich Porphyry. These results show that apatite from the ore-rich porphyries have slightly higher magmatic Cl-contents than those from the ore-poor porphyries. This observation highlights the importance of magmatic chlorine content as an important factor in the magma fertility and in the development of an ore-rich porphyry intrusion.

5.4. Genetic model of the Buenavista del Cobre deposit

Based on cross-cutting relationships, zircon U-Pb geochronology and apatite geochemistry, we propose that the mineralization of Buenavista del Cobre deposit is the result of the emplacement of several porphyry intrusions within a period of at least 4 Ma (Fig. 14). Apatite geochemistry indicate that ore-poor and ore-rich porphyry intrusions record a different magmatic evolution. Indeed, all porphyry intrusions share similar magmatic oxidation states (as shown by the overlapping of apatite Eu and Ce anomalies; Fig. 11A) but exhibit differences in emplacement time, and apatite Sr and REE signatures (Fig. 11B and 12). We propose that these characteristics reflects changing petrogenetic processes through time.

The porphyry intrusions sequence probably began with the emplacement of the ore-poor Feldspar Porphyry at 59.7 ± 0.5/1.1 Ma (Fig. 14). Despite the lack of apatite in this porphyry because of acid alteration, we speculate that the injection of a hot, hydrous (>5.5 wt% H_2O) mafic magma into the upper crust during the early stages of the magmatic system may have promoted the crystallization of high temperature hydrated minerals as hornblendes in the absence of plagioclase fractionation, which crystallizes at lower temperatures (e.g., Loucks, 2014; Fig. 14). As previously discussed, this process can remove some of the H_2O volume (retained in the crystals) of the residual magma, resulting in a subsequent ore-poor porphyry intrusion. In porphyry copper systems, it is common for the early porphyry intrusions to be poorly mineralized and for the well-mineralized porphyries to develop at later stages of the magmatic evolution (e.g., El Salvador; Gustafson and Hunt, 1975; Lee et al., 2017).

At Buenavista del Cobre, we suspect that as the temperature of the parental magma (Tinaja-Cuitaca Batholith) decreases with inward crystallization and magma differentiation in a closed system, there was a change in magma composition towards a more evolved composition, leading to plagioclase fractionation (Fig. 14). As plagioclase is an anhydrous mineral, this process allowed fluid exsolution and accumulation in the residual magma. At high temperature and pressure Cu is soluble in the fluid phase (Williams et al., 1995), as a result, porphyry copper melts issued from plagioclase-dominated fractional crystallization tend to produce ore-rich porphyry intrusions. Cross-cutting relationships indicate that a period of Cu-Mo fertility began after the emplacement of the Feldspar Porphyry, associated with the emplacement of the ore-rich La Colorada Porphyry at 58.9 ± 0.5/1.0 Ma (Fig. 14). In addition, the ore-rich 755 Porphyry probably represent another magmatic pulse with an emplacement age of 57.5 ± 0.2/0.9 Ma as this crystallization age does not overlap with the mineralization age of the La Colorada breccia pipe (Fig. 10). Apatite geochemistry in both intrusions indicates plagioclase fractionation, which explains their ore-rich character (Fig. 14). Moreover, anhydrous mineral fractionation can promote H_2O but also a volatile content increase in the residual magma. This is evidenced by the high apatite Cl content of the La Colorada and 755 porphyry intrusions (Fig. 9). As these ore-rich porphyries

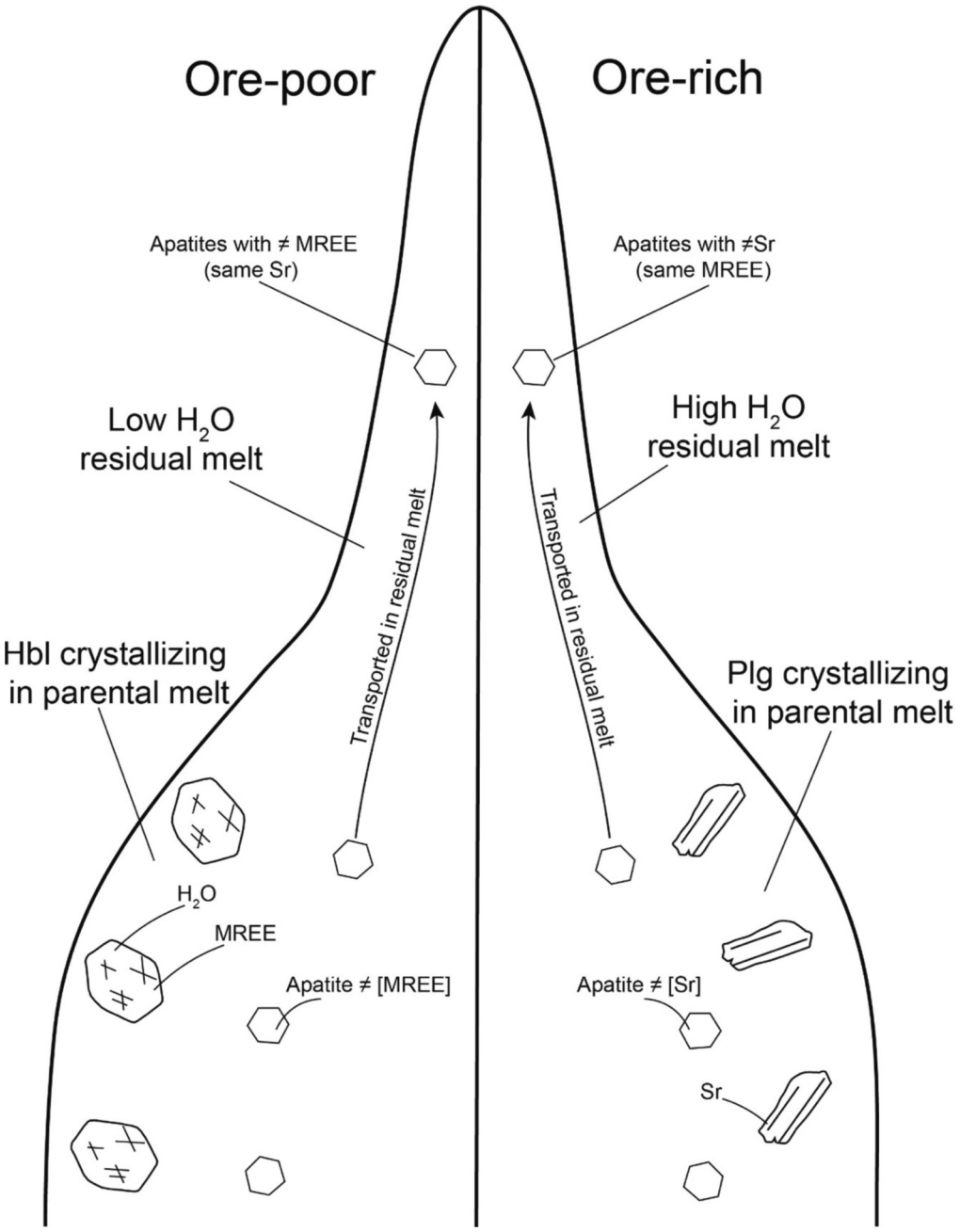

Fig. 13. Timing of apatite crystallization relative to hornblende and plagioclase fractionation in the parental magma of ore-poor vs ore-rich porphyries. Apatite co-crystallizing with hornblende exhibit a wide range in MREE concentrations (≠[MREE]), the residual magma present low H_2O content, impeding metal transportation and promoting the formation of an ore-poor porphyry. When plagioclase, which preferentially incorporates Sr, crystallizes at the same time as apatite, the latter show a wide range in their Sr content (≠[Sr]). As plagioclase is an anhydrous mineral, its crystallization leads to a H_2O content increase and favors Cu solubility in the residual melt leading to the formation of ore-rich porphyry magmas. Note that in this model, apatite crystals crystallized at depth and are transported to shallower crustal levels at the time of the porphyry emplacement (as indicated by the occurrence of apatite as sub-rounded inclusions in the major minerals of the porphyry rocks).

are not separated by a known ore-poor porphyry, we consider that their emplacement time correspond to a long period of Cu-Mo productivity at the Buenavista del Cobre deposit (Fig. 14). Interestingly, at the Mariquita porphyry copper deposit (Fig. 1) which has estimated resources of about 58 Mt of Cu at 0.4–0.6 % (Aponte-Barrera, 2009), the age of mineralization has been constrained by two Re-Os molybdenite ages between 59.2 ± 0.3 Ma and 59.3 ± 0.3 Ma (Del Rio-Salas et al., 2017). These mineralization ages are in good agreement with the timing of the mineralization (~59 Ma) associated with the La Colorada porphyry emplacement and suggest a productive period of Cu-Mo mineralization at the batholitic scale.

At 56.5 ± 0.3/0.9 Ma, the ore-poor 8–110 Porphyry was emplaced. This intrusion is characterized by an apatite geochemical signature indicating hornblende fractionation at depth (Fig. 12). Moreover, the low Cl content of apatite in this intrusion (Fig. 9) is in good agreement with its ore-poor character as a low-Cl magma composition implies a limited metal transport capacity in the exsolved fluids as there are less chlorine complexes available (Shinohara, 1994; Williams et al., 1995). We thus propose that the 8–110 intrusion followed a magmatic recharge of the batholith (and probably magma mixing?) at ~ 57 Ma, and the

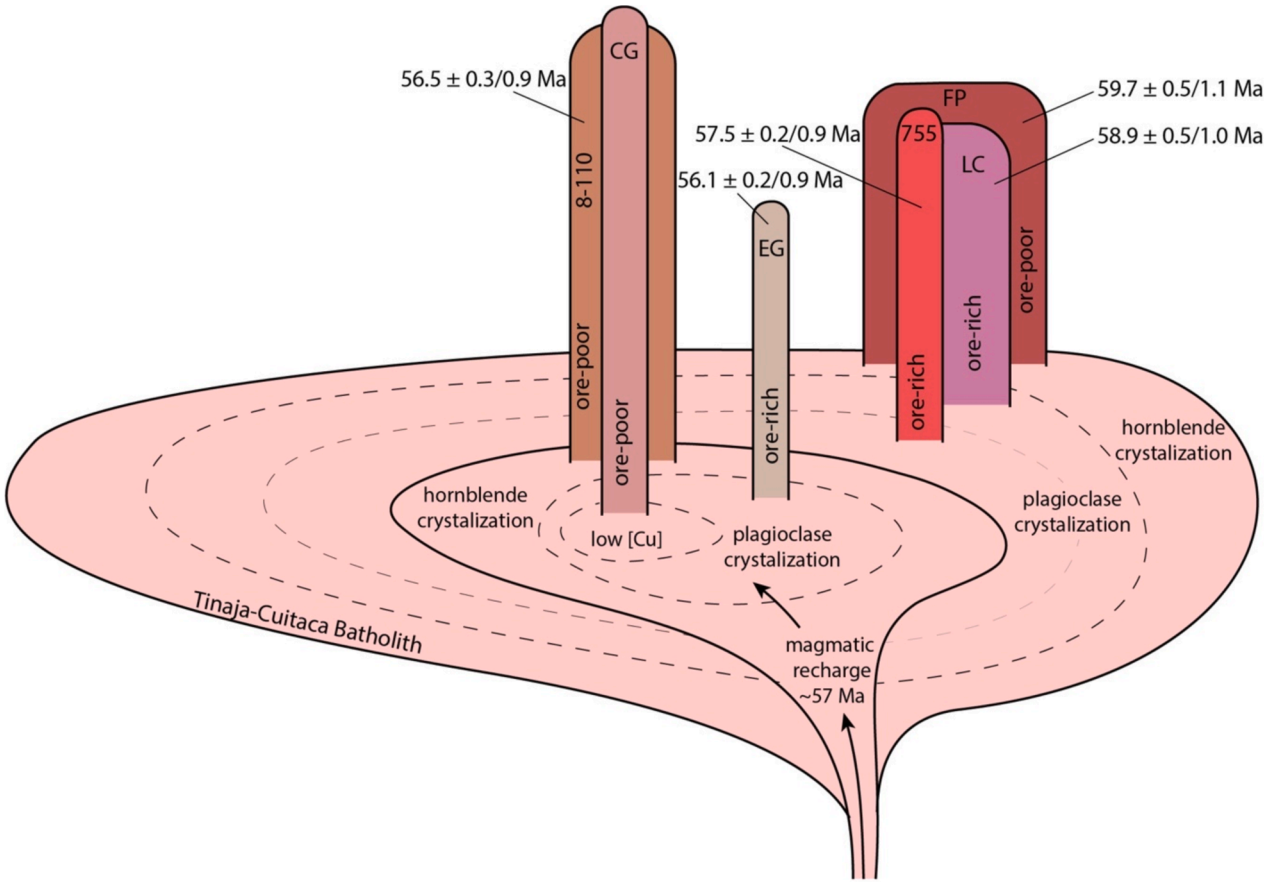

Fig. 14. Petrogenetic model for the formation of the Buenavista del Cobre porphyry copper deposit. A first magmatic cycle involving hornblende partial crystallization followed by plagioclase partial crystallization produced a sequence of ore-poor and ore-rich porphyry intrusions represented by the Feldspar Porphyry (FP), and La Colorada (LC) and 755 porphyries, respectively. A magmatic recharge of the batholith at ca. 57 Ma triggered a new sequence of ore-poor followed by ore-rich porphyries intrusions corresponding to the 8–110 Porphyry and El Galo Porphyry (EG), respectively. The end of the magmatic-hydrothermal system is marked by the emplacement of the ore-poor Coarse-grained Porphyry (CG), the scarce sulfide mineralization in this intrusion reflecting the fluids and metals exhaustion at the end of the magmatic cycle.

beginning of a new magmatic cycle (Fig. 14). This recharge triggered the resumption of hornblende crystallization at depth. After a period of fractional crystallization from which the 8–110 ore-poor Porphyry was produced, a new period of Cu-Mo productivity began when the evolving batholithic magma composition allowed plagioclase fractionation. Increased H_2O exsolution triggered the emplacement of the ore-rich El Galo Porphyry at 56.1 ± 0.2/0.9 Ma (Fig. 14), characterized by apatite with relatively high Cl content (Fig. 9). We propose that the end of the magmatic-hydrothermal system is marked by the emplacement of the ore-poor Coarse-grained Porphyry (Fig. 14). We interpret the absence of Cu mineralization associated with the emplacement of this intrusion as reflecting the fluids and metals exhaustion at the end of the magmatic cycle (Fig. 14).

6. Conclusions

The Buenavista del Cobre porphyry Cu-Mo deposit is the result of the superposition of multiple magmatic-hydrothermal pulses over a period of at least 4 Ma. The proposed genetic model involves two cycles of supply, cooling and partial crystallization of the parental magma of the porphyry intrusions and gives new insights on the petrogenetic processes at the origin of porphyry magma fertility. Fractional crystallization process of the parental magma influences the fertility of the porphyry magmas, resulting in the formation of ore-rich or ore-poor porphyry intrusions. The evolution of the parental melt by fractional crystallization of plagioclase increases the H_2O content of the residual magma resulting in the formation of ore-rich porphyritic intrusions. In contrast, hornblende fractionation leads to the formation of ore-poor porphyritic intrusions.

The variations of apatite REE signatures (such as $(Ce/Yb)_N$ and $(La/Sm)_N$ ratios) and trace element composition (such as Sr and Cl, U and Th) can be used to track petrogenetic processes involved in the formation of an economic porphyry copper deposit. This contribution further supports that petrogenetic processes controlling porphyry copper magmas fertility are recorded in the composition of apatite at a deposit scale and highlights the importance of considering apatite geochemistry as an exploration tool.

In addition, the recognition of the Cananea granite below the present-day pit at Buenavista del Cobre deposit indicates that the skarn Zn-Cu mineralization hosted in the Paleozoic sequence might be present below the Mesa and Henrietta Formations in the eastern part of the deposit. Finally, the confirmation of the presence of the Cordilleran Jurassic magmatic arc at Cananea latitudes increases the possibility of finding undiscovered Jurassic magmatic-hydrothermal systems in the Cananea Mining District.

Declaration of competing interest

The authors declare the following financial interests/personal relationships which may be considered as potential competing interests: Victor Salvador Almada-Gutiérrez reports a relationship with Grupo Mexico that includes: travel reimbursement. Edgardo Barrera-Moreno

reports a relationship with Grupo Mexico that includes: employment. If there are other authors, they declare that they have no known competing financial interests or personal relationships that could have appeared to influence the work reported in this paper.

Acknowledgments

VAG thanks CONAHCYT for a PhD grant (No. CVU: 852920). This study was partly funded by Grupo México through the PERUMEX project agreement between Grupo México and the Universidad Nacional Autónoma de México (UNAM). Travelling grants between Mexico and France were awarded by CONAHCYT, the ANUIES and the Comité ECOS-Nord through the project ECOS-Nord 322545 / M22U01. MN thanks the DGAPA-UNAM for funding the project PAPIIT IA105324 that partly funded field expanses. The authors especially thank Mario Rascón-Heimpel, Alfonso Martínez-Vera, and Cristo Bejarano-Carrillo for their help in securing funding. Sample preparation was supported by the LANGEM and we warmly thank E. González-Becuar and A. Orcí-Romero for their technical help. The authors thank Gaby Gutiérrez, Mario Quijada, Andrea Esparza, Mario Garcia, Alejandro Torres and Adolfo Gastélum of the geological department of the Buenavista del Cobre mine for provided guidance and valuable help during field work. The authors also wish to thank the Editor-in-Chief Dr. Huayong Chen, associate editor Dr. Bo Xu, Dr. Max Verdugo-Ihl and two anonymous reviewers for providing valuable reviews that greatly improved the manuscript.

Appendix A. Supplementary data

Supplementary data to this article can be found online at https://doi.org/10.1016/j.oregeorev.2024.106320.

Data availability

All raw data are in supplementary materials

References

Anderson, T.H., Rodríguez-Castañeda, J.L. and Silver, L.T. (2005). Jurassic rocks in Sonora, Mexico—relations to the Mojave- Sonora megashear and its inferred northwestward extension, in Anderson, T.H.; McKee, J.W.; y Steiner, M.B., eds., The Mojave-Sonora megashear hypothesis: development, assessment, and alternatives: *Geological Society of America Special Paper* 393, 51–95. https://doi.org/10.1130/0-8137-2393-0.51}.

Anderson, T.H., Silver, L.T., 1977. U-Pb isotope ages of granitic plutons near Cananea. Sonora. *Economic Geology* 72 (5), 827–836. https://doi.org/10.2113/gsecongeo.72.5.827.

Anderson, T.H., Silver, L.T., 1981. An overview of Precambrian rocks in Sonora. Revista Mexicana De Ciencias Geológicas 5 (2), 131–139.

Aponte-Barrera, M., 2009. Geología y mineralización del yacimiento Mariquita, distrito de Cananea: In Clark, K.F., Salas-Pizá, G.A., Cubillas-Estrada, R. (eds.): Geología Económica de México: Servicio Geológico Mexicano, p. 852–856.

Ayala-Fontes, 2009. Geología y mineralización en el distrito minero Cananea, Sonora, México. In: Clark, K.F., Salas-Pizá, G.A., Cubillas-Estrada, R. (Eds.), Geología Económica de México. Servicio Geológico Mexicano, pp. 804–810.

Ballard, J.R., Palin, J.M., Williams, I.S., Campbell, I.H., Faunes, A., 2001. Two ages of porphyry intrusion resolved for the super-giant Chuquicamata copper deposit of northern Chile by ELA-ICP-MS and SHRIMP. Geology 29 (5), 383–386. https://doi.org/10.1130/0091-7613(2001)029<0383:TAOPIR>2.0.CO;2.

Barra, F., Ruiz, J., Valencia, V.A., Ochoa-Landín, L., Chesley, J.T., Zurcher, L., 2005. Laramide porphyry Cu-Mo mineralization in northern Mexico: Age constraints from Re-Os geochronology in molybdenite. Econ. Geol. 100 (8), 1605–1616. https://doi.org/10.2113/gsecongeo.100.8.1605.

Barrat, J.A., Zanda, B., Moynier, F., Bollinger, C., Liorzou, C., Bayon, G., 2012. Geochemistry of CI chondrites: Major and trace elements, and Cu and Zn isotopes. Geochim. Cosmochim. Acta 83, 79–92. https://doi.org/10.1016/j.gca.2011.12.011.

Barton, M.D., Girardi, J.D., Kreiner, D.C., Seedorff, E., Zurcher, L., Dilles, J.H., Haxel, G., Johnson, D., 2011. Jurassic igneous-related metallogeny of southwestern North America. Reno, Nevada, Geological Society of Nevada, Great Basin Evolution and Metallogeny, pp. 373–396.

Belousova, E.A., Walters, S., Griffin, W.L., O'reilly, S.Y., 2001. Trace-element signatures of apatites in granitoids from the Mt Isa Inlier, northwestern Queensland. Aust. J. Earth Sci. 48 (4), 603–619. https://doi.org/10.1046/j.1440-0952.2001.00879.x.

Belousova, E.A., Griffin, W.L., O'Reilly, S.Y., Fisher, N.I., 2002. Apatite as an indicator mineral for mineral exploration: trace-element compositions and their relationship to host rock type. J. Geochem. Explor. 76 (1), 45–69. https://doi.org/10.1016/S0375-6742(02)00204-2.

Boehnke, P., Harrison, T.M., 2014. A meta-analysis of geochronologically relevant half-lives: what's the best decay constant? Int. Geol. Rev. 56 (7), 905–914. https://doi.org/10.1080/00206814.2014.908420.

Bouzari, F., Hart, C.J., Bissig, T., Barker, S., 2017. Hydrothermal alteration revealed by apatite luminescence and chemistry: A potential indicator mineral for exploring covered porphyry copper deposits. Econ. Geol. 111 (6), 1397–1410. https://doi.org/10.2113/econgeo.111.6.1397.

Brass, G.W., Mattes, B.W., Reid, R.P., Whitman, J.M., 1983. Mesozoic interaction of the Kula Plate and the western margin of North America. Tectonophysics 99 (2–4), 231–239. https://doi.org/10.1016/0040-1951(83)90105-1.

Bruand, E., Fowler, M., Storey, C., Darling, J., 2017. Apatite trace element and isotope applications to petrogenesis and provenance. Am. Mineral. 102 (1), 75–84. https://doi.org/10.2138/am-2017-5744.

Bushnell, S.E., 1988. Mineralization at Cananea, Sonora, and the paragenesis and zoning of breccia pipes in quartzofeldspathic rock. Econ. Geol. 83 (8), 1760–1781. https://doi.org/10.2113/gsecongeo.83.8.1760.

Cao, M., Li, G., Qin, K., Seitmuratova, E.Y., Liu, Y., 2012. Major and trace element characteristics of apatites in granitoids from Central Kazakhstan: implications for petrogenesis and mineralization. Resour. Geol. 62 (1), 63–83. https://doi.org/10.1111/j.1751-3928.2011.00180.x.

Chelle-Michou, C., Chiaradia, M., 2017. Amphibole and apatite insights into the evolution and mass balance of Cl and S in magmas associated with porphyry copper deposits. Contrib. Miner. Petrol. 172 (11), 105. https://doi.org/10.1007/s00410-017-1417-2/s00410-017-1417-2.

Chew, D.M., Petrus, J.A., Kamber, B.S., 2014a. U-Pb LA–ICPMS dating using accessory mineral standards with variable common Pb. Chem. Geol. 363, 185–199. https://doi.org/10.1016/j.chemgeo.2013.11.006.

Chew, D.M., Donelick, R.A., Donelick, M.B., Kamber, B.S., Stock, M.J., 2014b. Apatite chlorine concentration measurements by LA-ICP-MS. Geostand. Geoanal. Res. 38 (1), 23–35. https://doi.org/10.1111/j.1751-908X.2013.00246.x.

Cloos, M., 2001. Bubbling magma chambers, cupolas, and porphyry copper deposits. Int. Geol. Rev. 43 (4), 285–311. https://doi.org/10.1080/00206810109465015.

Cogné, N., Chew, D.M., Donelick, R.A., Ansberque, C., 2020. LA-ICP-MS apatite fission track dating: A practical zeta-based approach. Chem. Geol. 531, 119302. https://doi.org/10.1016/j.chemgeo.2019.119302.

Cogné, N., Derycke, A., Gallagher, K., 2024. The McClure Mountain Syenite Apatite as a Potential Age Control Reference Material for LA-ICP-MS AFT and U-Pb Double Dating. Geostand. Geoanal. Res. https://doi.org/10.1111/ggr.12545.

Coney, P.J., Harms, T.A., 1984. Cordilleran metamorphic core complexes: Cenozoic extensional relics of Mesozoic compression. Geology 12 (9), 550–554. https://doi.org/10.1130/0091-7613(1984)12<550:CMCCCE>2.0.CO;2.

Coney, P.J., Reynolds, S.J., 1977. Cordilleran benioff zones. Nature 270 (5636), 403–406. https://doi.org/10.1038/270403a0.

Corfu, F., Hanchar, J.M., Hoskin, P.W., Kinny, P., 2003. Atlas of zircon textures. Rev. Mineral. Geochem. 53 (1), 469–500. https://doi.org/10.2113/0530469.

Correa-García, J. P. (1983). Distribución del molibdeno en el distrito minero de Cananea, Sonora. Universidad de Sonora, Tesis de licenciatura (65 pp.).

Cox, D. P., Miller, R. J., and Woodbourne, K. L. (2006). The Laramide Mesa Formation and the Ojo de Agua Caldera, Southeast of the Cananea Copper Mining District, Sonora, Mexico. US Geological Survey.

Damon, P.E., Mauger, R.L., 1966. Epeirogeny-orogeny viewed from the Basin and Range province. Trans Am Inst Min Metall Engrs 235, 99–112.

Del Rio-Salas, R., Ochoa-Landín, L., Ruiz, J., Eastoe, C., Meza-Figueroa, D., Zuñiga-Hernández, H., Mendívil-Quijada, H., Quintanar-Ruiz, F., 2013. Geology, stable isotope, and U-Pb geochronology of the Mariquita porphyry copper and Lucy Cu–Mo deposits, Cananea District, Mexico: a contribution to regional exploration. J. Geochem. Explor. 124, 140–154. https://doi.org/10.1016/j.gexplo.2012.08.016.

Del Rio-Salas, R., Ochoa-Landín, L., Valencia-Moreno, M., Calmus, T., Meza-Figueroa, D., Salgado-Souto, S., Kirk, J., Ruiz, J., Mendívil-Quijada, H., 2017. New U-Pb and Re–Os geochronology of Laramide porphyry copper mineralization along the Cananea lineament, northeastern Sonora, Mexico: Contribution to the understanding of the Cananea copper district. Ore Geol. Rev. 81, 1125–1136. https://doi.org/10.1016/j.oregeorev.2015.11.029.

Drewes, H., 1971. Mesozoic stratigraphy of the Santa Rita Mountains, southeast of Tucson, Arizona. U.S. Geol. Surv. Prof. Pap. 658-C, 81 pp.

Eisele, J., Isachsen, C.E., 2001. Crustal growth in southern Arizona: U-Pb geochronologic and Sm-Nd isotopic evidence for addition of the Paleoproterozoic Cochise block to the Mazatzal Province. American Journal of Earth Sciences 310, 773–797. https://doi.org/10.2475/AJS.301.9.773.

Emmons, S.F., 1910. Cananea mining district of Sonora. Mexico. *Economic Geology* 5 (4), 312–356. https://doi.org/10.2113/gsecongeo.5.4.312.

Engebretson, D.C., Cox, A., Gordon, R.G., 1985. Relative motions between oceanic and continental plates in the Pacific basin. Geological Society of America Special Paper 206, 1–59. https://doi.org/10.1130/SPE206-p1.

Farfán-Panamá, J.L., 2002. Caracterización de los yacimientos en Skarn de Buenavista en Cananea. Universidad de Sonora, tesis de maestría, Son, p. 113.

Ferrari, L., Orozco-Esquivel, T., Bryan, S.E., Lopez-Martinez, M., Silva-Fragoso, A., 2018. Cenozoic magmatism and extension in western Mexico: Linking the Sierra Madre Occidental silicic large igneous province and the Comondú Group with the Gulf of California rift. Earth Sci. Rev. 183, 115–152. https://doi.org/10.1016/j.earscirev.2017.04.006.

Gans, P.B., 1997. Large-magnitude Oligo-Miocene extension in southern Sonora: Implications for the tectonic evolution of northwest Mexico. Tectonics 16 (3), 388–408. https://doi.org/10.1029/97TC00496.

Gastil, R.G., Morgan, G.J., Krummenacher, D., 1978. Mesozoic History of Peninsular California and Related Areas East of the Gulf of California. in *Mesozoic Paleogeography of the Western United States: Pacific Section, Society of Economic Paleontologists and Mineralogists, Pacific Coast Paleogeography Symposium* Vol. 2, 107–116.

Gustafson, L.B., Hunt, J.P., 1975. The porphyry copper deposit at El Salvador. Chile. *Economic Geology* 70 (5), 857–912. https://doi.org/10.2113/gsecongeo.70.5.857.

Harris, A.C., Allen, C.M., Bryan, S.E., Campbell, I.H., Holcombe, R.J., Palin, J.M., 2004. ELA-ICP-MS U-Pb zircon geochronology of regional volcanism hosting the Bajo de la Alumbrera Cu–Au deposit: implications for porphyry-related mineralization. Miner. Deposita 39, 46–67. https://doi.org/10.1007/s00126-003-0381-0.

Harris, A.C., Dunlap, W.J., Reiners, P.W., Allen, C.M., Cooke, D.R., White, N.C., Campbell, I.H., Golding, S.D., 2008. Multimillion year thermal history of a porphyry copper deposit: application of U-Pb, 40 Ar/39 Ar and (U–Th)/He chronometers, Bajo de la Alumbrera copper–gold deposit, Argentina. Miner. Deposita 43, 295–314. https://doi.org/10.1007/s00126-007-0151-5.

Horstwood, M.S., Košler, J., Gehrels, G., Jackson, S.E., McLean, N.M., Paton, C., Pearson, N.J., Sircombe, K., Sylvester, P., Vermeesch, P., Bowring, J.F., Condon, D.J., Schoene, B., 2016. Community-derived standards for LA-ICP-MS U-(Th-) Pb geochronology–Uncertainty propagation, age interpretation and data reporting. Geostand. Geoanal. Res. 40 (3), 311–332. https://doi.org/10.1111/j.1751-908X.2016.00379.x.

Jackson, S.E., Pearson, N.J., Griffin, W.L., Belousova, E.A., 2004. The application of laser ablation-inductively coupled plasma-mass spectrometry to in situ U-Pb zircon geochronology. Chem. Geol. 211 (1–2), 47–69. https://doi.org/10.1016/j.chemgeo.2004.06.017.

Jochum, K.P., Weis, U., Stoll, B., Kuzmin, D., Yang, Q., Raczek, I., Jacob, D.R., Stracke, A., Birbaum, K., Frick, D.A., Günther, D., Enzweiler, J., 2011. Determination of reference values for NIST SRM 610–617 glasses following ISO guidelines. Geostand. Geoanal. Res. 35 (4), 397–429. https://doi.org/10.1111/j.1751-908X.2011.00120.x.

Keith, S.B., Swan, M.M., 1995. Tectonic setting, petrology, and genesis of the Laramide porphyry copper cluster of Arizona, Sonora, and New Mexico. Porphyry Copper Deposits of the American Cordillera: Arizona Geological Society Digest 20, 339–346.

Klemme, S., John, T., Wessels, M., Kusebauch, C., Berndt, J., Rohrbach, A., Schmid-Beurmann, P., 2013. Synthesis of trace element bearing single crystals of Chlor-Apatite (Ca 5 (PO 4) 3 Cl) using the flux growth method. Chem. Cent. J. 7, 1–6. https://doi.org/10.1186/1752-153X-7-56.

Lang, J.R., Titley, S.R., 1998. Isotopic and geochemical characteristics of Laramide magmatic systems in Arizona and implications for the genesis of porphyry copper deposits. Econ. Geol. 93 (2), 138–170. https://doi.org/10.2113/gsecongeo.93.2.138.

Lee, C.T.A., Bachmann, O., 2014. How important is the role of crystal fractionation in making intermediate magmas? Insights from Zr and P systematics. Earth Planet. Sci. Lett. 393, 266–274. https://doi.org/10.1016/j.epsl.2014.02.044.

Lee, R.G., Dilles, J.H., Tosdal, R.M., Wooden, J.L., Mazdab, F.K., 2017. Magmatic evolution of granodiorite intrusions at the El Salvador porphyry copper deposit, Chile, based on trace element composition and U/Pb age of zircons. Econ. Geol. 112 (2), 245–273. https://doi.org/10.2113/econgeo.112.2.245.

Leveille, R.A., Stegen, R.J., 2012. "The Southwestern North America Porphyry Copper Province", Geology and Genesis of Major Copper Deposits and Districts of the World: A Tribute to Richard H. Sillitoe, Jeffrey W. Hedenquist, Michael Harris, Francisco Camus. Society of Economic Geologists Special Publication 16, 361–401. https://doi.org/10.5382/SP.16.15.

Loader, M. (2017). Mineral indicators of porphyry Cu fertility. (Doctoral dissertation, Imperial College London) (436 pp.).

Lodders, K., 2010. Solar system abundances of the elements. In *Principles and Perspectives in Cosmochemistry: Lecture Notes of the Kodai School on'Synthesis of Elements in Stars' held at Kodaikanal Observatory*. Springer, Berlin Heidelberg, pp. 379–417.

Loucks, R.R., 2014. Distinctive composition of copper-ore-forming arc magmas. Aust. J. Earth Sci. 61 (1), 5–16. https://doi.org/10.1080/08120099.2013.865676.

Maksaev, V., Munizaga, F., McWilliams, M., Fanning, M., Mathur, R., Ruiz, J., and Zentilli, M. (2004). New chronology for El Teniente, Chilean Andes, from U-Pb, 40Ar/39Ar, Re-Os, and fission-track dating: Implications for the evolution of a supergiant porphyry Cu-Mo deposit. In: Sillitoe, R. H., Perelló, J., & Vidal, C. E. (Eds.) Andean Metallogeny: New Discoveries, Concepts, and Updates, *Society of Economic Geologists, 11,* pp. 15-54. https://doi.org/10.5382/SP.11.02.

Mao, M., Rukhlov, A.S., Rowins, S.M., Spence, J., Coogan, L.A., 2016. Apatite trace element compositions: A robust new tool for mineral exploration. Econ. Geol. 111 (5), 1187–1222. https://doi.org/10.2113/econgeo.111.5.1187.

McDowell, F.W., Roldán-Quintana, J., Amaya-Martínez, R., 1997. Interrelationship of sedimentary and volcanic deposits associated with Tertiary extension in Sonora. Mexico. *Geological Society of America Bulletin* 109 (10), 1349–1360. https://doi.org/10.1130/0016-7606(1997)109<1349:IOSAVD>2.3.CO;2.

McDowell, F.W., Roldán-Quintana, J., Connelly, J.N., 2001. Duration of Late Cretaceous–early Tertiary magmatism in east-central Sonora. Mexico. *Geological Society of America Bulletin* 113 (4), 521–531. https://doi.org/10.1130/0016-7606(2001)113<0521:DOLCET>2.0.CO;2.

McDowell, F.W., McIntosh, W.C., Farley, K.A., 2005. A precise 40Ar–39Ar reference age for the Durango apatite (U–Th)/He and fission-track dating standard. Chem. Geol. 214 (3–4), 249–263. https://doi.org/10.1016/j.chemgeo.2004.10.002.

Meinert, L.D., 1980. Skarn, manto, and breccia pipe formation in sedimentary rocks in the Cananea District. Stanford University, Sonora, Mexico, p. 232. Unpublished PhD dissertation.

Meinert, L.D., 1982. Skarn, manto, and breccia pipe formation in sedimentary rocks of the Cananea mining district, Sonora. Mexico. *Economic Geology* 77 (4), 919–949. https://doi.org/10.2113/gsecongeo.77.4.919.

Nathwani, C.L., Loader, M.A., Wilkinson, J.J., Buret, Y., Sievwright, R.H., Hollings, P., 2020. Multi-stage arc magma evolution recorded by apatite in volcanic rocks. Geology 48 (4), 323–327. https://doi.org/10.1130/G46998.1.

Nathwani, C.L., Wilkinson, J.J., Brownscombe, W., John, C.M., 2023. Mineral texture classification using deep convolutional neural networks: an application to zircons from porphyry copper deposits. e2022JB025933 J. Geophys. Res. Solid Earth 128 (2). https://doi.org/10.1029/2022JB025933.

Noguez-Alcántara, B. (2008). Reconstrucción del modelo genético y evolución tectónica del yacimiento tipo pórfido cuprífero Milpillas, Distrito de Cananea, Sonora, Mexico: Hermosillo, Sonora, Mexico, Posgrado en Ciencias de la Tierra, Universidad Nacional Autónoma de México. *Unpublished Ph. D. Thesis, Universidad Nacional Autónoma de México, (390 pp.)*.

Nosenzo, F., Manzotti, P., Poujol, M., Ballèvre, M., Langlade, J., 2022. A window into an older orogenic cycle: P-T conditions and timing of the pre-Alpine history of the Dora-Maira Massif (Western Alps). J. Metam. Geol. 40 (4), 789–821. https://doi.org/10.1111/jmg.12646.

Nourse, J.A., Anderson, T.H., Silver, L.T., 1994. Tertiary metamorphic core complexes in Sonora, northwestern Mexico. Tectonics 13 (5), 1161–1182. https://doi.org/10.1029/93TC03324.

Ochoa-Landín, L., Echávarri-Pérez, A., 1978. Observaciones preliminares sobre la secuencia de las intrusiones hipabisales en el Tajo Colorada-veta del distrito minero de Cananea. Universidad de Sonora. Boletín Del Departamento De Geología, Hermosillo, México, pp. 57–60.

Ochoa-Landín, L., Navarro-Mayer, A., 1979. Historia geológica y tectónica del distrito de Cananea y alteración y mineralización de los tajos Colorada-Veta y Kino: Universidad de Sonora. Boletín Del Departamento De Geología 2 (2), 150–184.

Ortiz-Olvera, V., 2022. Estudio petrográfico, geoquímico y estructural del depósito de tipo skarn de Buenavista zinc. Universidad Nacional Autónoma de México. Tesis de maestría, Cananea, Sonora, p. 161.

Pan, L.C., Hu, R.Z., Wang, X.S., Bi, X.W., Zhu, J.J., Li, C., 2016. Apatite trace element and halogen compositions as petrogenetic-metallogenic indicators: Examples from four granite plutons in the Sanjiang region, SW China. Lithos 254, 118–130. https://doi.org/10.1016/j.lithos.2016.03.010.

Paton, C., Hellstrom, J., Paul, B., Woodhead, J., Hergt, J., 2011. Iolite: Freeware for the visualisation and processing of mass spectrometric data. J. Anal. At. Spectrom 26 (12), 2508–2518. https://doi.org/10.1039/C1JA10172B.

Perry, V.D., 1935. Copper deposits of the Cananea district Sonora, Mex. In *Sixteenth International Geol. Congress, Copper Resources of*. WORLD Vol. 1, 413–418.

Perry, V.D., 1961. The Significance of Mineralized Breccia Pipes: Mining Eng. 13, 367–376.

Piccoli, P.M., Candela, P.A., 2002. Apatite in igneous systems. Rev. Mineral. Geochem. 48 (1), 255–292. https://doi.org/10.2138/rmg.2002.48.6.

Proffett, J.M., 2003. Geology of the Bajo de la Alumbrera porphyry copper-gold deposit. Argentina. *Economic Geology* 98 (8), 1535–1574. https://doi.org/10.2113/gsecongeo.98.8.1535.

Prowatke, S., Klemme, S., 2006. Trace element partitioning between apatite and silicate melts. Geochim. Cosmochim. Acta 70 (17), 4513–4527. https://doi.org/10.1016/j.gca.2006.06.162.

Quan, Y., Yang, D., Yan, X., Wang, A., Hao, L., Yang, H., Wang, F., Xu, W., 2023. Petrogenesis of Mesozoic granitoids in the northeastern North China Craton: Constraints from apatite trace elements and in-situ Nd isotopic data. Lithos 450, 107190. https://doi.org/10.1016/j.lithos.2023.107190.

Reynolds, P., Ravenhurst, C., Zentilli, M., Lindsay, D., 1998. High-precision 40Ar/39Ar dating of two consecutive hydrothermal events in the Chuquicamata porphyry copper system. Chile. *Chemical Geology* 148 (1–2), 45–60. https://doi.org/10.1016/S0009-2541(97)00129-0.

Richards, J.P., 2003. Tectono-magmatic precursors for porphyry Cu-(Mo-Au) deposit formation. Econ. Geol. 98 (8), 1515–1533. https://doi.org/10.2113/gsecongeo.98.8.1515.

Richards, J.P., 2011. High Sr/Y arc magmas and porphyry Cu±Mo±Au deposits: Just add water. Econ. Geol. 106 (7), 1075–1081. https://doi.org/10.2113/econgeo.106.7.1075.

Rodríguez-Castañeda, J.L., and Anderson, T.H. (2011). El arco magmático jurásico en Sonora, México — Distribución, edades y ambiente tectónico, *in* Calmus, Thierry, ed., Panorama de la geología de Sonora, México: Universidad Nacional Autónoma de México, *Instituto de Geología, Boletín 118(*4), 81–111.

Santillana-Villa, C., Valencia-Moreno, M., Del Rio-Salas, R., Ochoa-Landín, L., 2021. Geochemical variations of precursor and ore-related intrusive rocks associated with porphyry copper deposits in Sonora, northwestern Mexico. J. S. Am. Earth Sci. 105, 102823. https://doi.org/10.1016/j.jsames.2020.102823.

Schoene, B., Bowring, S.A., 2006. U-Pb systematics of the McClure Mountain syenite: thermochronological constraints on the age of the 40 Ar/39 Ar standard MMhb. Contributions to Mineralogy and Petrology 151, 615–630. https://doi.org/10.1007/s00410-006-0077-4.

Schwartz, G.M., 1947. Hydrothermal alteration in the" porphyry copper" deposits. Econ. Geol. 42 (4), 319–352. https://doi.org/10.2113/gsecongeo.42.4.319.

Sha, L.K., Chappell, B.W., 1999. Apatite chemical composition, determined by electron microprobe and laser-ablation inductively coupled plasma mass spectrometry, as a probe into granite petrogenesis. Geochim. Cosmochim. Acta 63 (22), 3861–3881. https://doi.org/10.1016/S0016-7037(99)00210-0.

Shinohara, H., 1994. Exsolution of immiscible vapor and liquid phases from a crystallizing silicate melt: Implications for chlorine and metal transport. Geochim. Cosmochim. Acta 58 (23), 5215–5221. https://doi.org/10.1016/0016-7037(94)90306-9.

Sillitoe, R.H., 2010. Porphyry Copper Systems. *Economic Geology* 105 (1), 3–41. https://doi.org/10.2113/gsecongeo.105.1.3.

Singer, D. A., Berger, V. I., and Moring, B. C. (2005). Porphyry copper deposits of the world: database, map, and grade and tonnage models. *US Geological Survey open-file report*, 2005, *1060*(9).

Sláma, J., Košler, J., Condon, D.J., Crowley, J.L., Gerdes, A., Hanchar, J.M., Horstwood, S.A., Morris, G.A., Nasdala, L., Norberg, N., Schaltegger, U., Schoene, B., Tubrett, M.N., Whitehouse, M.J., 2008. Plešovice zircon—a new natural reference material for U-Pb and Hf isotopic microanalysis. Chem. Geol. 249 (1–2), 1–35. https://doi.org/10.1016/j.chemgeo.2007.11.005.

Sonder, L.J., Jones, C.H., 1999. Western United States extension: How the west was widened. Annu. Rev. Earth Planet. Sci. 27 (1), 417–462. https://doi.org/10.1146/annurev.earth.27.1.417.

Stewart, J.H., 1988. Latest Proterozoic and Paleozoic southern margin of North America and the accretion of Mexico. Geology 16 (2), 186–189. https://doi.org/10.1130/0091-7613(1988)016<0186:LPAPSM>2.3.CO;2.

Stock, J., Molnar, P., 1988. Uncertainties and implications of the Late Cretaceous and Tertiary position of North America relative to the Farallon, Kula, and Pacific plates. Tectonics 7 (6), 1339–1384. https://doi.org/10.1029/TC007i006p01339.

Sun, C.Y., Cawood, P.A., Xu, W.L., Zhang, X.M., Tang, J., Li, Y., Sun, Z., Xu, T., 2022. In situ geochemical composition of apatite in granitoids from the eastern Central Asian Orogenic Belt: A window into petrogenesis. Geochim. Cosmochim. Acta 317, 552–573. https://doi.org/10.1016/j.gca.2021.10.028.

Thomson, S.N., Gehrels, G.E., Ruiz, J., Buchwaldt, R., 2012. Routine low-damage apatite U-Pb dating using laser ablation–multicollector–ICPMS. Geochem. Geophys. Geosyst. 13, 1–23. https://doi.org/10.1029/2011GC003928.

Tosdal, R. M., and Richards, J. P. (2001). Magmatic and structural controls on the development of porphyry Cu ± Mo ± Au deposits. In: Richards, J.P., Tosdal, R.M. (Eds.), Structural Controls on Ore Genesis: Society of Economic Geologists. Reviews in Economic Geology vol. 14, pp. 157-181. https://doi.org/10.5382/Rev.14.06.

Tosdal, R.M., Haxel, G.B., Wright, J.E., Jenney, J.P., Reynolds, S.J., 1989. Jurassic geology of the Sonoran Desert region, southern Arizona, southeastern California, and northernmost Sonora: Construction of a continental-margin magmatic arc. Geologic Evolution of Arizona: Arizona Geological Society Digest 17, 397–434.

Valencia, V.A., Noguez-Alcántara, B., Barra, F., Ruiz, J., Gehrels, G., Quintanar, F., Valencia-Moreno, M., 2006. Re-Os molybdenite and LA-ICPMS-MC U-Pb zircon geochronology for the Milpillas porphyry copper deposit: insights for the timing of mineralization in the Cananea District, Sonora. Mexico. *Revista Mexicana De Ciencias Geológicas* 23 (1), 39–53.

Valencia-Moreno, M., Camprubí, A., Ochoa-Landín, L., Calmus, T., Mendívil-Quijada, H., 2016. Latest Cretaceous-early Paleogene "boom" of porphyry Cu mineralization associated with the Laramide magmatic arc of Mexico. Ore Geol. Rev. 81, 1113–1124. https://doi.org/10.1016/j.oregeorev.2016.05.005.

Valencia-Moreno, M., López-Martínez, M., Orozco-Esquivel, T., Ferrari, L., Calmus, T., Noury, M., Mendívil-Quijada, H., 2021. The Cretaceous-Eocene Mexican Magmatic Arc: Conceptual framework from geochemical and geochronological data of plutonic rocks. Earth Sci. Rev. 103721. https://doi.org/10.1016/j.earscirev.2021.103721.

Valencia-Moreno, M., González-León, C.M., Solari, L., Rascón-Heimpel, M.A., González-Becuar, E., Lozano-Santacruz, R., Pérez-Arvizu, O., 2024. U-Pb zircon geochronology and geochemistry of the Jurassic magmatic rocks from the region of Cananea and Nacozari, northeastern Sonora, Mexico: timing and composition of the southernmost edge of the Jurassic continental arc. Can. J. Earth Sci. 61 (1), 117–133. https://doi.org/10.1139/cjes-2023-0059.

Valentine, W.G., 1936. Geology of the Cananea Mountains, Sonora, Mexico. Bull. Geol. Soc. Am. 47 (1), 53–86. https://doi.org/10.1130/GSAB-47-53.

Varela, F. E. (1972). *Tourmaline in the Cananea mining district, Sonora, Mexico: Unpub.* M. S. Thesis, University of California, Berkeley, 79 p.

Vega-Granillo, R., Calmus, T., 2003. Mazatan metamorphic core complex (Sonora, Mexico): structures along the detachment fault and its exhumation evolution. J. S. Am. Earth Sci. 16 (4), 193–204. https://doi.org/10.1016/S0895-9811(03)00066-X.

Vermeesch, P., 2018. IsoplotR: A free and open toolbox for geochronology. Geosci. Front. 9 (5), 1479–1493. https://doi.org/10.1016/j.gsf.2018.04.001.

Virtue, T.L., 1996. Geology, mineralogy, and genesis of supergene enrichment at the Cananea porphyry copper deposit, Sonora. Mexico. Unpublished M.Sc, Thesis, The University of Texas at El Paso, p. 284.

Wernicke, B., 1992. Cenozoic extensional tectonics of the US Cordillera. The Geology of North America 3, 553–582. https://doi.org/10.1130/DNAG-GNA-G3.553.

Whitmeyer, S.J., Karlstrom, K., 2007. Tectonic model for the Proterozoic growth of North America. Geosphere 3 (4), 220–259. https://doi.org/10.1130/GES00055.1.

Williams, T.J., Candela, P.A., Piccoli, P.M., 1995. The partitioning of copper between silicate melts and two-phase aqueous fluids: an experimental investigation at 1 kbar, 800 C and 0.5 kbar, 850 C. Contrib. Miner. Petrol. 121, 388–399. https://doi.org/10.1007/s004100050104.

Wodzicki, W.A., 2001. The evolution of magmatism and mineralization in the Cananea district, Sonora, Mexico. Special Publication-Society of Economic Geologists 8, 243–264. https://doi.org/10.5382/SP.08.15.

Wodzicki, W. A. (1995). *The evolution of Laramide igneous rocks and porphyry copper mineralization in the Cananea district, Sonora, Mexico.* Unpublished PhD dissertation, University of Arizona, Tucson, pp. 181.

Wones, D.R., 1989. Significance of the assemblage titanite+ magnetite+ quartz in granitic rocks. Am. Mineral. 74 (7–8), 744–749.

Wong, M.S., Gans, P.B., 2003. Tectonic implications of early Miocene extensional unroofing of the Sierra Mazatán metamorphic core complex, Sonora. Mexico. *Geology* 31 (11), 953–956. https://doi.org/10.1130/G19843.1.

Wong, M.S., Gans, P.B., Scheier, J., 2010. The 40Ar/39Ar thermochronology of core complexes and other basement rocks in Sonora, Mexico: Implications for Cenozoic tectonic evolution of northwestern Mexico. *Journal of Geophysical Research: Solid.* Earth 115 (B7). https://doi.org/10.1029/2009JB007032.

Zhang, X., Guo, F., Zhang, B., Zhao, L., Wu, Y., Wang, G., Alemayehu, M., 2020. Magmatic evolution and post-crystallization hydrothermal activity in the early Cretaceous Pingtan intrusive complex, SE China: Records from apatite geochemistry. Contrib. Miner. Petrol. 175, 1–18. https://doi.org/10.1007/s00410-020-1675-2.